Stochastic processes dominate the within and between host evolution of influenza virus

Running Title: Influenza dynamics within and between hosts

John T. McCrone[1], Robert J. Woods[2], Emily T. Martin[3], Ryan E. Malosh[3], Arnold S. Monto[3], and Adam S. Lauring[1,2 *]

[1] Department of Microbiology and Immunology, University of Michigan, Ann Arbor, MI 48109

[2] Division of Infectious Diseases, Department of Internal Medicine, University of Michigan, Ann Arbor, MI 48109

[3] Department of Epidemiology, University of Michigan, Ann Arbor, MI 48109

* Corresponding author

Adam S. Lauring

1150 W. Medical Center Dr.

MSRB1 Room 5510B

Ann Arbor, MI 48109-5680

(734) 764-7731

alauring@med.umich.edu

Abstract Word Count:

Main Text Word Count:

Key Words – influenza virus, bottleneck, transmission, diversity, evolution

Abstract

The global evolutionary dynamics of influenza virus ultimately derive from processes that take place within and between infected individuals. Here we define the dynamics of influenza A virus populations in human hosts through next generation sequencing of 249 specimens from 200 individuals collected over 6290 person-seasons of observation. Because these viruses were collected over 5 seasons from individuals in a prospective community-based cohort, they are broadly representative of natural human infections with seasonal viruses. We used viral sequence data from 35 serially sampled individuals to estimate a within host effective population size of 30-70 and an in vivo mutation rate of $4x10^{-5}$ per nucleotide per cellular infectious cycle. These estimates are consistent across several models and robust to the models' underlying assumptions. We also identified 43 epidemiologically linked and genetically validated transmission pairs. Maximum likelihood optimization of multiple transmission models estimates an effective transmission bottleneck of 1-2 distinct genomes. Our data suggest that positive selection of novel viral variants is inefficient at the level of the individual host and that genetic drift and other stochastic processes dominate the within and between host evolution of influenza A viruses.

Introduction

The rapid evolution of influenza viruses has led to reduced vaccine efficacy, widespread drug resistance, and the continuing emergence of novel strains. Broadly speaking, evolution is the product of deterministic processes, such as selection, and stochastic processes, such as genetic drift (Kouyos et al. 2006). The relative contribution of each is greatly affected by the effective population size, or size of an idealized population whose dynamics are similar to that of the population in question (Rouzine et al. 2001). If the effective population size of a virus is large, as in quasispecies models, evolution is largely deterministic and the frequency of a mutation can be predicted based on its starting frequency and selection coefficient. In small populations,

selection is inefficient, and changes in mutation frequency are strongly influenced by migration or genetic drift.

Viral dynamics may differ across spatial and temporal scales, and a complete understanding of influenza evolution requires studies at all levels (Nelson & Holmes 2007; Holmes 2009) .The global evolution of influenza A virus (IAV) is dominated by the positive selection of novel antigenic variants that circulate in the tropics and subsequently seed annual epidemics in the Northern and Southern hemisphere (Rambaut et al. 2008). Whole genome sequencing has also demonstrated the importance of intrasubtype reassortment to the emergence of diverse strains that differ in their antigenicity. While continual positive selection of antigenically drifted variants drives global patterns, whole genome sequencing of viruses on more local scales suggests the importance of stochastic processes such as strain migration and within-clade reassortment (Nelson et al. 2006).

It is now feasible to efficiently sequence patient-derived isolates at sufficient depth of coverage to define the diversity and dynamics of virus evolution within individual hosts (Kao et al. 2014). Studies of IAV populations in animal and human systems suggest that most intrahost single nucleotide variants (iSNV) are rare and that intrahost populations are subject to strong purifying selection (Rogers et al. 2015; Murcia et al. 2010; Iqbal et al. 2009; Poon et al. 2016; Dinis et al. 2016; Debbink et al. 2017). While positive selection of adaptive variants is commonly observed in cell culture (Doud et al. 2017; ARCHETTI & HORSFALL 1950; Foll et al. 2014), it has only been documented within human hosts in the extreme cases of drug resistance (Gubareva et al. 2001; Ghedin et al. 2011; Rogers et al. 2015), long-term infection of immunocompromised hosts (Xue et al. 2017) or experimental infections with attenuated viruses (Sobel Leonard et al. 2016). Indeed, we and others have been unable to identify evidence for positive selection in natural

52 human infections (Debbink et al. 2017; Dinis et al. 2016), and its relevance to within host
53 processes is unclear.
54
55 Despite limited evidence for positive selection, it is clear that novel mutations do arise within
56 hosts. Their potential for subsequent spread through host populations is determined by the size
57 of the transmission bottleneck (Alizon et al. 2011; Zwart & Elena 2015). If the transmission
58 bottleneck is sufficiently wide, low frequency variants can plausibly be transmitted and spread
59 through host populations (Geoghegan et al. 2016). Because the transmission bottleneck is
60 conceptually similar to the effective population size between hosts, its size will also inform the
61 relative importance of selection and genetic drift in determining which variants are transmitted.
62 While experimental infections of ferrets suggest a very narrow transmission bottleneck (Varble
63 et al. 2014; Wilker et al. 2013), studies of equine influenza support a bottleneck wide enough to
64 allow transmission of rare iSNV (Hughes et al. 2012; Murcia et al. 2010). The only available
65 genetic study of influenza virus transmission in humans estimated a remarkably large
66 transmission bottleneck, allowing for transmission of 100-200 genomes (Poon et al. 2016; Sobel
67 Leonard et al. 2017).
68
69 Here, we use next generation sequencing of within host influenza virus populations to define the
70 evolutionary dynamics of influenza A viruses (IAV) within and between human hosts. We apply
71 a benchmarked analysis pipeline to identify iSNV and to characterize the genetic diversity of
72 H3N2 and H1N1 populations collected over five post-pandemic seasons from individuals
73 enrolled in a prospective household study of influenza. We use these data to estimate the *in*
74 *vivo* mutation rate and the within and between host effective population size. We find that
75 intrahost populations are characterized by purifying selection, a small effective population size,
76 and limited positive selection. Contrary to what has been previously reported for human
77 influenza transmission (Poon et al. 2016), but consistent with what has been observed in other

viruses (Zwart & Elena 2015), we identify a very tight effective transmission bottleneck that limits the transmission of rare variants.

Results

We used next generation sequencing to characterize influenza virus populations collected from individuals enrolled in the Household Influenza Vaccine Effectiveness (HIVE) study (Monto et al. 2014; Ohmit et al. 2013; Ohmit et al. 2015; Ohmit et al. 2016; Petrie et al. 2013), a community-based cohort that enrolls 213-340 households of 3 or more individuals in Southeastern Michigan each year (Table 1). These households are followed prospectively from October to April, with symptom-triggered collection of nasal and throat swab specimens for identification of respiratory viruses by RT-PCR (see Methods). In contrast to case-ascertained studies, which identify households based on an index case who seeks medical care, the HIVE study identifies symptomatic individuals regardless of illness severity. In the first four seasons of the study (2010-2011 through 2013-2014), respiratory specimens were collected 0-7 days after illness onset. Beginning in the 2014-2015 season, each individual provided two samples, a self-collected specimen at the time of symptom onset and a clinic-collected specimen obtained 0-7 days later. Each year, 59-69% of individuals had self-reported or confirmed receipt of that season's vaccine prior to local circulation of influenza virus.

Over five seasons and nearly 6,290 person-seasons of observation, we identified 77 cases of influenza A/H1N1pdm09 infection and 313 cases of influenza A/H3N2 infection (Table 1). Approximately half of the cases (n=166) were identified in the 2014-2015 season, in which there was an antigenic mismatch between the vaccine and circulating strains (Flannery et al. 2016). All other seasons were antigenically matched. Individuals within a household were considered an epidemiologically linked transmission pair if they were both positive for the same subtype of

103 influenza virus within 7 days of each other. Several households had 3 or 4 symptomatic cases
104 within this one-week window, suggestive of longer chains of transmission (Table 1).
105
106 *Within host populations have low genetic diversity*
107 We processed all specimens for viral load quantification and next generation sequencing. Viral
108 load measurements (genome copies per µl) were used for quality control in variant calling,
109 which we have shown is highly sensitive to input titer (McCrone & Lauring 2016) (Figure 1A).
110 Accordingly, we report data on 249 high quality specimens from 200 individuals, which had a
111 viral load of $>10^3$ copies per microliter of transport media, adequate RT-PCR amplification of all
112 eight genomic segments, and an average read coverage of $>10^3$ across the genome (Table 1,
113 Supplementary Figure 1).
114
115 We identified intrahost single nucleotide variants (iSNV) using our empirically validated analysis
116 pipeline (McCrone & Lauring 2016). Our approach relies heavily on the variant caller DeepSNV,
117 which uses a clonal plasmid control to distinguish between true iSNV and errors introduced
118 during sample preparation and/or sequencing (Gerstung et al. 2012). Given the diversity of
119 influenza viruses that circulate locally each season, there were a number of instances in which
120 our patient-derived samples had mutations that were essentially fixed (>0.95 frequency) relative
121 to the clonal control. DeepSNV is unable to estimate an error rate for the control or reference
122 base at these positions. We therefore performed an additional benchmarking experiment to
123 identify a threshold for majority iSNV at which we could correctly infer whether or not the
124 corresponding minor allele was also present (see Methods). We found that we could correctly
125 identify a minor allele at a frequency of ≥2% when the frequency of the major allele was ≤98%.
126 We therefore report data on iSNV present at frequencies between 2 and 98%. As expected, this
127 threshold improved the specificity of our iSNV identification and decreased our sensitivity to

detect variants below 5% compared to our initial validation experiment (McCrone & Lauring 2016), which did not employ a frequency threshold (Supplementary Table 1).

Consistent with our previous studies and those of others, we found that the within host diversity of human influenza A virus (IAV) populations is low (Poon et al. 2016; Dinis et al. 2016; Debbink et al. 2017; Sobel Leonard et al. 2016; McCrone & Lauring 2016). Two hundred forty-three out of the 249 samples had fewer than 10 minority iSNV (median 2, IQR 1-3). There were 6 samples with greater than 10 minority iSNV. In 3 of these cases, the frequency of iSNVs were tightly distributed about a mean suggesting that the iSNV were linked and that the samples represented mixed infections. Consistent with this hypothesis, putative genomic haplotypes based on these minority iSNV clustered with distinct isolates on phylogenetic trees (Supplementary Figures 2 and 3). While viral shedding was well correlated with days post symptom onset (Figure 1A) the number of minority iSNV identified was not affected by the day of infection, viral load, subtype, or vaccination status (Figure 1B and Supplementary Figure 4).

The vast majority of minority variants were rare (frequency 0.02-0.07), and iSNV were distributed evenly across the genome (Figure 1C and 1D). The ratio of nonsynonymous to synonymous variants was 0.64 and was never greater than 1 in any 5% bin, which suggests that within host populations were under purifying selection. We also found that minority variants were rarely shared among multiple individuals. Ninety-five percent of minority iSNV were only found once, 4.7% were found in 2 individuals, and no minority iSNV were found in more than 3 individuals. The low level of shared diversity suggests that within host populations were exploring distinct regions of sequence space with little evidence for parallel evolution. Of the 31 minority iSNV that were found in multiple individuals (triangles in Figure 1D), 4 were nonsynonymous.

Although the full range of the H3 antigenic sites have not been functionally defined, it is estimated that 131 of the 329 amino acids in HA1 lie in or near these sites (Lee & Chen 2004). We identified 17 minority nonsynonymous iSNV in these regions (Supplementary Table 2). Six of these were in positions that differ among antigenically drifted viruses (Smith et al. 2004; Wiley et al. 1981), and two (193S and 189N) lie in the "antigenic ridge" that is a major contributor to drift (Koel et al. 2013). Three of these have been detected at the global level as consensus variants since the time of isolation (128A, 193S and 262N) with two (193S and 262N) seemingly increasing in global frequency (Neher & Bedford 2015) (Supplementary Figure 5). Additionally, we identified 1 putative H1N1 antigenic variant (208K in C_a) (Caton et al. 1982; Xu et al. 2010). In total, putative antigenic variants account for 1.0-2.5% of minority iSNV identified and were found in 3.5-8.0% of infections. None of these iSNV were shared among multiple individuals.

Estimation of effective population size

Given the above observations, we hypothesized that within host populations of IAV are under purifying selection and that variants that rise to detectable levels do so by a neutral process as opposed to positive selection. Consistent with this hypothesis, we found that nonsynonymous and synonymous iSNV exhibited similar changes in frequency over time in the 35 individuals who provided serial specimens that contained iSNV (Figure 2A and 2B). We used a maximum likelihood approach to estimate the within host effective population size (N_e) of IAV by fitting a diffusion approximation of the Wright-Fisher model (Kimura 1955). This model assumes that changes in iSNV frequency are due solely to random genetic drift and not selection, that iSNV are independent of one another, and that the effective population is sufficiently large to justify a continuous approximation to changes in allele frequency. The diffusion approximation of the Wright-Fisher model assigns probabilities to frequency changes given an N_e and the number of generations between sample times. In our model we fixed the within host generation time as either 6 or 12 hours (Geoghegan et al. 2016) and report the findings for the 6 hour generation

time below. We then asked what population size makes the observed changes in frequency most likely (Figure 2B). We restricted this analysis to samples taken at least 1 day apart (n = 29), as there was very little change in iSNV frequency in populations sampled twice on the same day (R^2 = 0.986, Figure 2B and Supplementary Figure 6). The concordance of same day samples suggests that our sampling procedure is reproducible and that less than a generation had passed between samplings. Maximum likelihood optimization of this diffusion model revealed a within host effective population size of 35 (95% CI 26-46, Table 2).

The diffusion approximation makes several simplifying assumptions, which if violated could influence our findings. To ensure our results were robust to the assumption of a large population, we employed a discrete interpretation of the Wright-Fisher model which makes no assumptions about population size (Williamson & Slatkin 1999). In this case we found an effective population size of 32 (95% CI 28-41), very close to our original estimate (Table 2). Both models assume complete independence of iSNV. To ensure this assumption did not affect our results, we fit the discrete model 1000 times, each time randomly subsetting our data such that only one iSNV per individual was included. This simulates a situation in which all modeled iSNV are independent and our assumption is met. Under these conditions we found a median effective population size of 33 (IQR 32-40), demonstrating negligible bias in the initial analysis due to correlation between iSNV.

As above, most iSNV in the longitudinal samples were rare (< 10%) and many became extinct between samplings. To ensure that our models were capable of accurately estimating the effective population size from such data, we simulated 1000 Wright-Fisher populations with iSNV present at approximately the same starting frequencies as in our data set and an N_e of 30, 50, or 100. In these simulations, we found mean N_e of 34, 56 and 117 (Figure 2C). These

simulations suggest that although this method may slightly overestimate the N_e, our results are not constrained by the data structure.

To this point, we have assumed that neutral processes are responsible for the observed changes in iSNV frequency within hosts. Although this assumption seems justified at least in part by the analysis above, we tested the robustness of our models by fitting the nonsynonymous (n = 27) and synonymous iSNV (n = 36) separately. Here, we estimated an effective population size of 30 using the nonsynonymous iSNV and an effective population size of 37 using the synonymous iSNV (Table 2). These estimates are very close to those derived from the whole dataset and suggest that nonsynonymous and synonymous mutations are influenced by similar within host processes. To further ensure that our results were not driven by a few outliers subject to strong selection, we ranked iSNV by their change in frequency over time and consecutively removed iSNV with the most extreme changes. We estimated the effective population size at each iteration and found that removing the top 50% most extreme iSNV only increased the effective population size to 161 (Figure 2D). Therefore, our estimates are robust to a reasonable number of non-neutral sites. Finally, we also applied a separate Approximate Bayesian Computational (ABC) method, which uses a non-biased moment estimator in conjunction with ABC to estimate the effective population size of a population as well as selection coefficients for the iSNV present (Foll et al. 2014). This distinct approach relaxes the previous assumption regarding neutrality. We applied this analysis to the 16 longitudinal pairs that were sampled 1 day apart and estimated an effective population of 69. We were unable to reject neutrality for just 7 of the 35 iSNV in this data set (Figure 2E). These seven mutations consisted of 3 nonsynonymous and 4 synonymous mutations and were split between two individuals. None were putative antigenic variants.

Identification of forty-three transmission pairs

231 We analyzed virus populations from 85 households with concurrent infections to quantify the
232 level of shared viral diversity and to estimate the size of the IAV transmission bottleneck (Table
233 1). Because epidemiological linkage does not guarantee that concurrent cases constitute a
234 transmission pair (Petrie et al. 2017), we used a stringent rubric to eliminate individuals in a
235 household with co-incident community acquisition of distinct viruses. We considered all
236 individuals in a household with symptom onset within a 7-day window to be epidemiologically
237 linked. The donor in each putative pair was defined as the individual with the earlier onset of
238 symptoms. We discarded a transmission event if there were multiple possible donors with the
239 same day of symptom onset. Donor and recipients were not allowed to have symptom onset on
240 the same day, unless the individuals were both index cases for the household. In these 6
241 instances, we analyzed the data for both possible donor-recipient directionalities. Based on
242 these criteria, our cohort had 124 putative household transmission events over 5 seasons
243 (Table 1). Of these, 52 pairs had samples of sufficient quality for reliable identification of iSNV
244 from both individuals.
245
246 We next used sequence data to determine which of these 52 epidemiologically linked pairs
247 represented true household transmission events as opposed to coincident community-acquired
248 infections. We measured the genetic distance between influenza populations from each
249 household pair by L1-norm and compared these distances to those of randomly assigned
250 community pairs within each season (Figure 3A, see also trees in Supplementary Figures 2 and
251 3). While the L1-norm of a pair captures differences between the populations at all levels, in our
252 cohort, it was largely driven by differences at the consensus level. We only considered
253 individuals to be a true transmission pair if they had a genetic distance below the 5th percentile
254 of the community distribution of randomly assigned pairs (Figure 3A). Forty-seven household
255 transmission events met this criterion (Figure 3B). Among these 47 sequence-validated
256 transmission pairs, 3 had no iSNV in the donor and 1 additional donor appeared to have a

mixed infection. These four transmission events were removed from our bottleneck analysis as donors without iSNV are uninformative and mixed infections violate model assumptions of site independence (see Methods). We estimated the transmission bottleneck in the remaining 43 high-quality pairs (37 H3N2, 6 H1N1, Figure 3B).

A transmission bottleneck restricts the amount of genetic diversity that is shared by both members of a pair. We found that few minority iSNV where polymorphic in both the donor and recipient populations (Figure 3C). Minority iSNV in the donor were either absent or fixed in the recipient (top and bottom of plot). The lack of shared polymorphic sites (which would lie in the middle of the plot in Figure 3C) suggests a stringent effective bottleneck in which only one allele is passed from donor to recipient.

Estimation of the transmission bottleneck

We applied a simple presence-absence model to quantify the effective transmission bottleneck in our cohort. The presence-absence model considers only whether or not a donor allele is present or absent in the recipient sample. Under this model, transmission is a neutral, random sampling process, and the probability of transmission is simply the probability that the iSNV will be included at least once in the sample given its frequency in the donor and the sample size, or bottleneck. We estimated a distinct bottleneck for each transmission pair and assumed these bottlenecks followed a zero-truncated Poisson distribution. This model also assumes that the sensitivity for detection of transmitted iSNVs is perfect and that each genomic site is independent of all others. We then used maximum likelihood optimization to determine the distribution of bottleneck sizes that best fit the data. We found a zero-truncated Poisson distribution with a mean of 1.66 (lambda = 1.12; 0.51-1.99, 95% CI) best described the data. This distribution indicates that the majority of bottlenecks are 1, and that very few are greater than 5 (probability 0.2%). There were no apparent differences between H3N2 and H1N1 pairs.

283 The model fit was evaluated by simulating each transmission event 1,000 times. The presence
284 or absence of each iSNV in the recipient was noted and the probability of transmission given
285 donor frequency determined. The range of simulated outcomes matched the data well, which
286 suggests that transmission is a selectively neutral event characterized by a stringent bottleneck
287 (Figure 3D).
288
289 The majority of transmitted iSNV were fixed in the recipients. Although this trend matches the
290 expectation given a small bottleneck, these data could also be consistent with a model in which
291 the probability of transmission is determined by the frequency at which iSNV are found at the
292 community level. To ensure our bottleneck estimates were an outcome of neutral transmission
293 and not an artifact of the larger community population structure or selection for the community
294 consensus, we created a null model by randomly assigning community "recipient-donor"
295 pairings. Each community "recipient" was drawn from the pool of individuals that were infected
296 after the "donor" but in the same season and with the same subtype as the donor. We then
297 identified whether or not each donor iSNV was found in the community recipient and determined
298 the relationship between "donor" frequency and probability of "transmission" for 1,000 such
299 simulations. Given the low level of diversity in our cohort, we predicted that rare iSNV would be
300 unlikely to be found in a random sample, while the major alleles should be fixed in most random
301 pairs. This trend is clearly demonstrated in Figure 3E. It is also clear that this null model fit the
302 data much more poorly than the presence/absence model, suggesting that the observed data in
303 our bona fide transmission pairs were not a product of community metapopulation structure, but
304 rather an outcome of neutral sampling events.
305
306 Because our bottleneck estimates were much lower than what has previously been reported for
307 human influenza (Poon et al. 2016), we investigated the impact that our simplifying assumptions
308 could have on our results. In particular, the presence-absence model assumes perfect detection

of variants in donor and recipient, and it can therefore underestimate the size of a bottleneck in the setting of donor-derived variants that are transmitted but not detected in the recipient. These "false negative" variants can occur when the frequency of an iSNV drifts below the level of detection (e.g. 2% frequency) or when the sensitivity of sequencing is less than perfect for variants at that threshold (e.g. 15% sensitivity for variants at a frequency 2-5%). To determine the impact of sequencing sensitivity and specificity on our bottleneck estimates, we re-called variants using our original pipeline without the 2% frequency cut-off. As shown in Supplementary Table 1, this increases the sensitivity of iSNV detection in the 1-5% frequency range, and also the number of false positive variant calls (McCrone & Lauring 2016). This analysis only slightly increased average transmission bottleneck to 2.10 (lambda = 1.67; 0.91-2.71, 95% CI), and indicates that our results are not biased by the added stringency used in the initial analysis (Supplementary Figures 7A and 7B).

To further investigate the impact of sequencing accuracy on our estimates, we inferred minor variants in our current pipeline (see above and methods) without a frequency cutoff. Ultimately, this reduced variant calling to a count method at a number of positions and greatly increased the number of shared minority iSNV in our samples (Supplementary Figure 7C). Many of these presumed false positive variant calls were at similar frequencies (0.1-2%) in donor and recipient. As such, the "apparent transmission" of rare variants drives an inflated estimate of the transmission bottleneck (118, see Supplementary Figure 7D). Simulation showed that this inflated bottleneck no longer fit the trend in the data, likely because the model is now forced to accommodate shared iSNV that are biased toward sequencing error as opposed to the actual transmission process.

We also estimated bottleneck size using a beta binomial model, which Leonard *et al.* have used to account for the stochastic loss of transmitted variants. This model allows for a limited amount

of time-independent genetic drift within the recipient (Sobel Leonard et al. 2017), and we modified it to also account for our benchmarked sensitivity for rare variants (Supplementary Table 1, Current Pipeline). For all donor-derived iSNV that were absent in the recipient, we estimated the likelihood that these variants were transmitted but either drifted below our level of detection or drifted below 10% and were missed by our variant identification. Despite the relaxed assumptions provided by this modified beta binomial model, maximum likelihood estimation only marginally increased the average bottleneck size (mean 1.73: lambda 1.22; 0.57-2.17, 95%CI) relative to the simpler presence-absence model. We simulated transmission and subsequent random drift using the beta binomial model and the estimated bottleneck distribution as above (Figure 3F). Although the model matched the data well, the fit was not better than that of the presence-absence model (AIC 83.0 for beta-binomial compared to 76.7 for the presence-absence model).

The mutation rate of influenza A virus within human hosts

The stringent influenza transmission bottleneck suggests that most infections are founded by one lineage and develop under essentially clonal processes. The diffusion approximation to the Wright-Fisher model (see above and Figure 2) can be used to predict the rate at which homogenous populations diversify from a clonal ancestor as a function of mutation rate and effective population size (Rouzine et al. 2001). Maximum likelihood optimization of this model suggested an *in vivo* neutral mutation rate of 4×10^{-6} mutations per nucleotide per replication cycle and a within host effective population size of 36 (given a generation time of 6 hours). These estimates are consistent with those above (Table 2). As we have recently estimated that 13% of mutations in influenza A virus are neutral (Visher et al. 2016), we estimated that the true *in vivo* mutation rate would be approximately 8 fold higher than our neutral rate – on the order of $3\text{-}4 \times 10^{-5}$. This in vivo mutation rate is close to our recently published estimate of influenza A

mutation rates in epithelial cells by fluctuation test (Pauly et al. 2017) and within the range of other estimates for IAV (Sanjuán et al. 2010).

Discussion

We find that seasonal influenza A viruses replicate within and spread among human hosts with very small effective population sizes. Because we used viruses collected over five influenza seasons from individuals enrolled in a prospective household cohort, these dynamics are likely to be broadly representative of many seasonal influenza infections in their natural transmission context. Our results are further strengthened by the use of a validated sequence analysis pipeline and models that are robust to the underlying assumptions. The small effective size of intrahost populations and the tight effective transmission bottleneck suggest that stochastic processes, such as genetic drift, dominate influenza virus evolution at the level of individual hosts. This stands in contrast to prominent role of positive selection in the global evolution of seasonal influenza.

While influenza virus populations are subject to continuous natural selection, selection is an inefficient driver of evolution in small populations (Rouzine et al. 2001). Despite a large viral copy number, our findings demonstrate that intrahost populations of influenza behave like much smaller populations. We therefore expect stochastic fluctuations to be the major force driving the fixation of novel variants within human hosts. This finding contradicts previous studies, which have found signatures of adaptive evolution in infected hosts (Gubareva et al. 2001; Rogers et al. 2015; Ghedin et al. 2011; Sobel Leonard et al. 2016). However, these studies rely on data from infections in which selective pressures are likely to be particularly strong (e.g. due to drug treatment or infection with a poorly adapted virus), or in which the virus has been allowed to propagate for extended periods of time (Xue et al. 2017). Under these conditions,

385 one can identify the action of positive selection on within host populations. We suggest that
386 these are important and informative exceptions to the drift regime defined here.
387
388 We used both a simple presence-absence model and a more complex beta binomial model to
389 estimate an extremely tight transmission bottleneck. The estimation of a small bottleneck size is
390 driven by low within-host diversity and very few minority iSNV shared among individuals in a
391 transmission pair. While our methods for variant calling may be more conservative than those
392 used in similar studies, we found that relaxing our variant calling criteria led to the inclusion of
393 false positive variants that inflated our estimates. Furthermore, the beta binomial model
394 accounts for false negative iSNV (i.e. variants that are transmitted but not detected in the donor),
395 which can lead to underestimated transmission bottlenecks (Sobel Leonard et al. 2017). Our
396 formulation of this model incorporates empirically determined sensitivity and specificity metrics
397 to account for both false negative iSNV and false positive iSNV (McCrone & Lauring 2016).
398 Finally, if rare, undetected, iSNV were shared between linked individuals, we would expect to
399 see transmission of more common iSNV (frequency 5-10%), which we can detect with high
400 sensitivity. In our data, the transmission probability iSNVs > 5% frequency in the donor were
401 also well predicted by small bottleneck size (Figure 3D).
402
403 Although the size of our transmission bottleneck is consistent with estimates obtained for other
404 viruses and in experimental animal models of influenza (Zwart & Elena 2015; Varble et al. 2014),
405 it differs substantially from the only other study of bottlenecks in natural human infection (Poon
406 et al. 2016; Sobel Leonard et al. 2017). While there are significant differences in the design and
407 demographics of the cohorts, the influenza seasons under study, and sequencing methodology
408 (Kugelman et al. 2017), the bottleneck size estimates are fundamentally driven by the amount of
409 viral diversity shared among individuals in a household. Importantly, we used both
410 epidemiologic linkage and the genetic relatedness of viruses in households to define

411 transmission pairs and to exclude confounding from the observed background diversity in the
412 community. We find that household transmission pairs and randomly assigned community pairs
413 had distinct patterns of shared consensus and minority variant diversity. The comparison to
414 random community pairs is important, as an unexplained aspect of the work of Poon et al. is
415 that rare iSNV were frequently shared by randomly selected individuals, and more common
416 ones were not (Poon et al. 2016).
417
418 Our estimates of IAV population dynamics are consistent across three separate models and
419 partitions of the data. The measurements of shared diversity are influenced by both between
420 and within host processes, and the transmission bottleneck is entirely consistent with the small
421 within host population size derived from the longitudinal samples. We also jointly estimated the
422 *in vivo* mutation rate and effective population size based on the frequency distribution of minor
423 alleles observed in the entire cohort. This model assumed a small transmission bottleneck,
424 produced a mutation rate that this consistent with previous estimates, and independently
425 reproduced the within host population size estimate. Given the concordance among these
426 distinct approaches, it is unlikely that our findings are biased by hidden assumptions or model
427 limitations.
428
429 Accurately modeling and predicting influenza virus evolution requires a thorough understanding
430 of the virus' population structure. Some models have assumed a large intrahost population and
431 a relatively loose transmission bottleneck (Geoghegan et al. 2016; Russell et al. 2012; Peck et
432 al. 2015). Here, adaptive iSNV can rapidly rise in frequency and low frequency variants can
433 have a high probability of transmission. In such a model, it would be possible for the highly
434 pathogenic H5N1 virus to develop the requisite 4-5 mutations to become transmissible through
435 aerosols during a single acute infection of a human host (Herfst et al. 2012; Russell et al. 2012).
436 Although the dynamics of emergent avian influenza and human adapted seasonal viruses likely

differ (Petrova & Russell 2017), our work suggests that fixation of multiple mutations over the course of a single acute infection is unlikely.

While it may seem counterintuitive that influenza evolution is dominated by drift on local scales and positive selection on global scales, these models are certainly not in conflict. Within individuals we have shown that the effective population is quite small, which suggests that selection is inefficient. Indeed, we have deeply sequenced 332 intrahost populations from 283 individuals collected over more than 11,000 person-seasons of observation and only identified a handful of minority antigenic variants with little evidence for positive selection (this work and (Debbink et al. 2017)). However, with several million infected individuals each year, even inefficient processes and rare events are likely to happen at a reasonable frequency on a global scale.

Methods

Description of the cohort

The HIVE cohort (Monto et al. 2014; Ohmit et al. 2013; Ohmit et al. 2015; Ohmit et al. 2016; Petrie et al. 2013), established at the UM School of Public Health in 2010, enrolled and followed households of at least 3 individuals with at least two children <18 years of age; households were then followed prospectively throughout the year for ascertainment of acute respiratory illnesses. Study participants were queried weekly about the onset of illnesses meeting our standard case definition (two or more of: cough, fever/feverishness, nasal congestion, sore throat, body aches, chills, headache if ≥3 yrs old; cough, fever/feverishness, nasal congestion/runny nose, trouble breathing, fussiness/irritability, decreased appetite, fatigue in <3 yrs old), and the symptomatic participants then attended a study visit at the research clinic on site at UM School of Public Health for sample collection. For the 2010-2011 through 2013-2014

seasons, a combined nasal and throat swab (or nasal swab only in children < 3 years of age) was collected at the onsite research clinic by the study team. Beginning with the 2014-2015 seasons, respiratory samples were collected at two time points in each participant meeting the case definition; the first collection was a self- or parent-collected nasal swab collected at illness onset. Subsequently, a combined nasal and throat swab (or nasal swab only in children < 3 years of age) was collected at the onsite research clinic by the study team. Families with very young children (< 3 years of age) were followed using home visits by a trained medical assistant.

Active illness surveillance and sample collection for cases were conducted October through May and fully captured the influenza season in Southeast Michigan in each of the study years. Data on participant, family and household characteristics, and on high-risk conditions were additionally collected by annual interview and review of each participant's electronic medical record. In the current cohort, serum specimens were also collected twice yearly during fall (November-December) and spring (May-June) for serologic testing for antibodies against influenza.

This study was approved by the Institutional Review Board of the University of Michigan Medical School, and all human subjects provided informed consent.

Identification of influenza virus

Respiratory specimens were processed daily to determine laboratory-confirmed influenza infection. Viral RNA was extracted (Qiagen QIAamp Viral RNA Mini Kit) and tested by RT-PCR for universal detection of influenza A and B. Samples with positive results by the universal assay were then subtyped to determine A(H3N2), A(H1N1), A(pH1N1) subtypes and B(Yamagata) and B(Victoria) lineages. We used primers, probes and amplification parameters developed by the Centers for Disease Control and Prevention Influenza Division for use on the

ABI 7500 Fast Real-Time PCR System platform. An RNAseP detection step was run for each specimen to confirm specimen quality and successful RNA extraction.

Quantification of viral load

Quantitative reverse transcription polymerase chain reaction (RT-qPCR) was performed on 5µl RNA from each sample using CDC RT-PCR primers InfA Forward, InfA Reverse, and InfA probe, which bind to a portion of the influenza M gene (CDC protocol, 28 April 2009). Each reaction contained 5.4µl nuclease-free water, 0.5µl each primer/probe, 0.5µl SuperScript III RT/Platinum Taq mix (Invitrogen 111732) 12.5µl PCR Master Mix, 0.1µl ROX, 5µl RNA. The PCR master mix was thawed and stored at 4°C, 24 hours before reaction set-up. A standard curve relating copy number to Ct value was generated based on 10-fold dilutions of a control plasmid run in duplicate.

Illumina library preparation and sequencing

We amplified cDNA corresponding to all 8 genomic segments from 5µl of viral RNA using the SuperScript III One-Step RT-PCR Platinum Taq HiFi Kit (Invitrogen 12574). Reactions consisted of 0.5µl Superscript III Platinum Taq Mix, 12.5µl 2x reaction buffer, 6µl DEPC water, and 0.2µl of 10µM Uni12/Inf1, 0.3µl of 10µM Uni12/Inf3, and 0.5µl of 10µM Uni13/Inf1 universal influenza A primers (Zhou et al. 2009). The thermocycler protocol was: 42˚C for 60 min then 94˚C for 2 min then 5 cycles of 94˚C for 30 sec, 44˚C for 30 sec, 68˚C for 3 min, then 28 cycles of 94˚C for 30 sec, 57˚C for 30 sec, 68˚C for 3 min. Amplification of all 8 segments was confirmed by gel electrophoresis, and 750ng of each cDNA mixture were sheared to an average size of 300 to 400bp using a Covaris S220 focused ultrasonicator. Sequencing libraries were prepared using the NEBNext Ultra DNA library prep kit (NEB E7370L), Agencourt AMPure XP beads (Beckman Coulter A63881), and NEBNext multiplex oligonucleotides for Illumina (NEB E7600S). The final concentration of each barcoded library was determined by Quanti PicoGreen dsDNA

quantification (ThermoFisher Scientific), and equal nanomolar concentrations were pooled. Residual primer dimers were removed by gel isolation of a 300-500bp band, which was purified using a GeneJet Gel Extraction Kit (ThermoFisher Scientific). Purified library pools were sequenced on an Illumina HiSeq 2500 with 2x125 nucleotide paired end reads. All raw sequence data have been deposited at the NCBI sequence read archive (BioProject submission ID: SUB2951236). PCR amplicons derived from an equimolar mixture of eight clonal plasmids, each containing a genomic segment of the circulating strain were processed in similar fashion and sequenced on the same HiSeq flow cell as the appropriate patient derived samples. These clonally derived samples served as internal controls to improve the accuracy of variant identification and control for batch effects that confound sequencing experiments.

Identification of iSNV

Intrahost single nucleotide variants were identified in samples that had greater than 10^3 genomes/µl and an average coverage >1000x across the genome. Variants were identified using DeepSNV and scripts available at https://github.com/lauringlab/variant_pipeline as described previously (McCrone & Lauring 2016) with a few minor and necessary modifications. Briefly, reads were aligned to the reference sequence (H3N2 2010-2011 & 2011-2012 : GenBank CY121496-503, H3N2 2012-2013:GenBank KJ942680-8, H3N2 2014-2015 : Genbank CY207731-8, H1N1 GenBank : CY121680-8) using Bowtie2 (35). Duplicate reads were then marked and removed using Picard (http://broadinstitute.github.io/picard/). We identified putative iSNV using DeepSNV. Bases with phred <30 were masked. Minority iSNV (frequency <50%) were then filtered for quality using our empirically determined quality thresholds (p-value <0.01 DeepSNV, average mapping quality >30, average Phred >35, average read position between 31 and 94). To control for PCR errors in samples with lower input titers, all isolates with titers between 10^3 and 10^5 genomes/µl were processed and sequenced in duplicate. Only iSNV that were found in both replicates were included in down stream analysis. The frequency of the

variant in the replicate with higher coverage at the iSNV location was assigned as the frequency of the iSNV. Finally, any SNV with a frequency below 2% was discarded.

Given the diversity of the circulating strain in a given season, there were a number of cases in which isolates contained mutations that were essentially fixed (>95%) relative to the plasmid control. Often in these cases, the minor allele in the sample matched the major allele in the plasmid control. We were, therefore, unable to use DeepSNV in estimating the base specific error rate at this site for these minor alleles and required an alternative means of eliminating true and false minority iSNV. To this end we applied stringent quality thresholds to these putative iSNV and implemented a 2% frequency threshold. In order to ensure we were not introducing a large number of false positive iSNV into our analysis, we performed the following experiment. Perth (H3N2) samples were sequenced on the same flow cell as both the Perth and Victoria (H3N2) plasmid controls. Minority iSNV were identified using both plasmid controls. This allowed us to identify rare iSNV at positions in which the plasmid controls differed both with and without the error rates provided by DeepSNV. We found that at a frequency threshold of 2% the methods were nearly identical (NPV of 1, and PPV of 0.94 compared to DeepSNV).

Overview of models for effective population size

We estimated the effective population size using two separate interpretations of a Wright-Fisher population (Ewens 2004). At its base, the Wright-Fisher model describes the expected changes in allele frequency of an ideal population, which is characterized by non-overlapping generations, no migration, no novel mutation, and no population structure. We then asked what size effective population would make the changes in frequency observed in our dataset most likely. We calculated these values using two applications of the Wright-Fisher model (i) a diffusion approximation (Kimura 1955)and (ii) a maximum likelihood approach based on the discrete interpretation (Williamson & Slatkin 1999).

For these estimates we restricted our analysis to longitudinal samples from a single individual that were separated by at least 1 day and only used sites that were polymorphic in the initial sample (29 of the 49 total serial sample pairs). We modeled only the iSNV that were the minor allele at the first time point, and we assumed a within host generation time of either 6 or 12 hours as proposed by Geoghegan *et al.* (Geoghegan et al. 2016).

Diffusion approximation

The diffusion approximation was first solved by Kimura in 1955 (Kimura 1955). This approximation to the discrete Wright-Fisher model has enjoyed widespread use in population genetics as it allows one to treat the random time dependent probability distribution of final allele frequencies as a continuous function (e.g. (Zanini et al. 2017; Kimura & Ohta 1969; Kimura 1971; Myers et al. 2008)). Here, we also included the limitations in our sensitivity to detect rare iSNV by integrating over regions of this probability density that were either below our limit of detection or within ranges where we expect less than perfect sensitivity as follows.

Let $P(p_0, p_t, t \mid N_e)$ be the time dependent probability of a variant drifting from an initial frequency of p_0 at time 0 p_t at time t generations given an effective population size of N_e where $0 < p_t < 1$.

The time dependent derivative of this probability has been defined using the Kolmogorov forward equation (Kimura 1955) and for haploid populations is:

$$P(p_0, p_t, t \mid N_e) = \sum_{i=1}^{\infty} p_0\, q_0 i(i+1)(2i+1) F(1-i, i+2, 2, p) \times F(1-i, i+2, 2, p_t) e^{-\left[\frac{i(i+1)}{2N_e}\right]t} \quad (1)$$

Where $q = 1 - p$ and F is the hypergeometric function. We approximated the infinite sum by summing over the first 50 terms. When we added an additional 50 terms (100 in total) we found no appreciable change in the final log likelihoods.

We denote the frequency of allele that is not observed at the second time point as $p_t \approx 0$ and the probability of such an event as $P(p_0, p_t \approx 0, t \mid N_e)$. This probability is given in equation 2 as the sum of the probability that the variant is truly lost by generation t (i.e. the other allele is fixed $P(q_0, q_t = 1, t \mid N_e)$), the probability that it is present but below the limit of detection (i.e. $P(p, p_t \approx 0, t \mid 0 < p_t < 0.02, N_e)$) and the probability the variant is not detected due to low sensitivity for rare variant detection (i.e. $P(p_0, p_t \approx 0, t \mid 0.02 < p_t < 0.1, N_e)$). The probability of not observing an allele at the second time is then

$$P(p_0, p_t \approx 0, t \mid N_e) = P(q_0, 1, t \mid N_e) + P(p, p_t \approx 0, t \mid 0 < p_t < 0.02, N_e) + P(p_0, p_t \approx 0, t \mid 0.02 < p_t < 0.1, N_e) \quad (2)$$

The first term in equation 2 is adapted from Kimura, 1955 as

$$P(q_0, 1, t \mid N_e) = q_0 + \sum_{i=1}^{\infty} (2i + 1) p_0 q_0 (-1)^i F(1 - i, i + 2, 2, q_0) e^{-[i(i+1)/2N_e]t} \quad (3)$$

Where q is defined as above. (Note that this is simply the probability of fixation for a variant at initial frequency q). As in equation 1 the infinite sum was approximated with a partial sum of 50 terms.

The probability of the allele drifting below our limit of detection can be found by integrating equation 1 between 0 and our limit of detection, 0.02. This was done numerically using the python package scipy.

$$P(p, p_t \approx 0, t \mid 0 < p_t < 0.02, N_e) = \int_0^{0.02} P\,(p_0, p_t, t|N_e)dp_t \quad (4)$$

Finally, the probability of an iSNV being present at the second time point, but escaping detection, is given by the integral of equation 1 between our benchmarked frequencies (0.02,0.05) times the false negative rate for that range. Here, we assumed the entire range had the same sensitivity as the benchmarked frequency at the lower bound and rounded recipient titers down to the nearest $\log_{10}$ titer (e.g. 10^3,10^4, 10^5). We also assumed perfect sensitivity above 10%.

$$P(p_0, p_t \approx 0, t \mid 0.02 < p_t < 0.1, N_e)) = \sum_{f_i}^{[0.02,0.05,0.10)} (\,\mathrm{FNR} \mid \mathrm{Titer}_r, f_i) \int_{f_i}^{f_{i+1}} P\,(p_0, p_t, t \mid N_e)dp_t \quad (5)$$

Where $(\mathrm{FNR} \mid \mathrm{Titer}_r, f_i)$ is the false negative rate given the frequency and the sample titer (See Supplemental Table 1) and $P(p_0, p_t, t \mid N_e)$ is defined in equation 1.

The log likelihood of an effective population size is the sum of the log of $P(p_0, p_t, t \mid N_e)$ for each minor allele in the data set, where either the position is polymorphic at time t (i.e. equation 1) or the allele is not observed at time t (i.e. equation 2).

Discrete Wright-Fisher estimation of N_e

The diffusion approximation treats changes in frequency as a continuous process because it assumes sufficiently large N_e. That assumption can be relaxed, and the effective population size

636 can be determined, by applying a maximum likelihood method developed by Williamsom and
637 Slatkin 1999 (Williamson & Slatkin 1999). In this model, the true allele frequencies move
638 between discrete states (i.e. the frequency must be of the form i/N_e where i is a whole number
639 in the range $[0, N_e]$. In the original application, allele counts were used, and sampling error was
640 added to the model as a binomial distribution with n determined by the sample size. Here, we
641 use the frequencies available from next generation sequencing and estimate sampling error as
642 a normal distribution with mean equal to the observed frequency and a standard deviation equal
643 to that observed in our benchmarking study for the 10^4 genomes/μl samples ($\sigma = 0.014$)
644 (McCrone & Lauring 2016).
645
646 In this model, the probability of observing an allele frequency shift from $\hat{p}_0$ to $\hat{p}_t$ in t generations
647 provided an effective population of N_e is the probability of observing $\hat{p}_0$ given some initial state
648 p_0 and the probability of the population having that state, times the probability of observing $\hat{p}_t$
649 given some final state p_t and the probability of moving from the initial to the final state summed
650 across all possible states.

$$P(p_0, p_t \mid N_e) = \sum^{p_0, p_t} P(\hat{p}_0 \mid p_0) P(p_0 \mid N_e) P(\hat{p}_t \mid p_t) P(p_t \mid p_0, N_e)$$

651 (6)
652
653 Where $\hat{p}_x$ are the observed probabilities and p_x are the real ones (of the form i/N_e discussed
654 above). The likelihood of observing a given frequency $\hat{p}_x$ given a defined state p_x is given by the
655 likelihood of drawing $\hat{p}_x$ from a normal distribution with mean p_x and standard deviation 0.014.
656

$$P(\hat{p}_x \mid p_x) = \mathrm{Norm}(p_x, 0.014)$$

657 (7)

As in Williamson and Slatkin 1999, we assume a uniform prior on the initial state. Because we know that our specificity is near perfect (above 2%, Supplemental Table 1) and we restrict our analysis to only polymorphic sites, the probability of any initial state is given by

$$P(p_0 \mid N_e) = \frac{1}{N_e - 1} \tag{8}$$

and finally the probability of moving from one state to another in t generations is given by

$$P(p_t, p_0 \mid N_e) = v_0 M^t v_t \tag{9}$$

Where M is a square transmission matrix with $N_e + 1$ rows and columns. Where $m_{i,j}$ is the probability of going from the ith configuration to the jth or the probability of drawing $j - 1$ out of binomial distribution with mean $(i - 1)/N_e$ and a sample size N_e. v_0 is a row vector of initial frequencies p_0 with 100% chance of initial state p_0, and v_t is column vector of the frequencies at time point t with 100% chance of the final state. In other words v_0 is a row vector of $N_e + 1$ states with 0 everywhere except in the ith position where $\frac{i-1}{N_e} = p_0$, and v_t is a column vector of $N_e + 1$ states with 0 everywhere except the jth position where $\frac{j-1}{N_e} = p_t$

Using the scalar and cumulative properties of matrix multiplication equation 6 reduces to

$$P(p_0, p_t \mid N_e) = [0, P(p_0 \mid q_{0_2})P(q_{0_2} \mid N_e), \ldots, P(p_0 \mid q_{0_{N_e-1}})P(q_{0_{N_e-1}} \mid N_e), 0] M^t \begin{bmatrix} P(p_t \mid q_{t_1}) \\ \vdots \\ P(p_t \mid q_{t_{N_e}}) \end{bmatrix} \tag{10}$$

677 The first and last entries in v_0 are 0 because we assume all measured sites represent
678 polymorphisms at the first time of sampling. As above, the log likelihood of a given population
679 size is then simply the sum of the log of $P(\hat{p}_0, \hat{p}_t, t \mid N_e)$ for each minor allele in the data set.
680
681 *Simulations*
682 To simulate within host evolution we set N_e in equation 10 to either 30, 50 or 100. For each
683 minor allele we used the closest available non-zero state given the effective population size as
684 the starting state. We then calculated the probability of moving to any other state and selected a
685 final state from this distribution. We then drew a final measured frequency from the normal
686 distribution to account for measurement errors.
687
688 *ABC model*
689 We estimated both the effective population size and selection coefficients using the approximate
690 Bayesian computation (ABC) described in (Foll et al. 2014) with the WFACB_v1.1 software
691 provided in (Foll et al. 2015). In its current implementation, this analysis requires the same time
692 points for each sample, and we restricted this analysis to longitudinal samples taken 1 day apart.
693 This subset constitutes 16 of the 29 modeled longitudinal samples. Briefly, we subsampled
694 polymorphic sites to 1,000x coverage to estimate allele counts from frequency data as in (Foll et
695 al. 2014). We then estimated the prior distribution of the effective population size using 10,000
696 bootstrap replicates. We selected a uniform distribution on the range [-0.5,0.5] as the prior
697 distribution for the selection coefficients. The posterior distributions were determined from
698 accepting the top 0.01% of 100,000 simulations.
699
700 *Overview of models used for estimating the transmission bottleneck*
701 We model transmission as a simple binomial sampling process (Sobel Leonard et al. 2017). In
702 our first model, we assume any transmitted iSNV, no matter the frequency, will be detected in

703 the recipient. In the second, we relax this assumption and account for false negative iSNV in the
704 recipient. To include the variance in the transmission bottlenecks between pairs we use
705 maximum likelihood optimization to fit the average bottleneck size assuming the distribution
706 follows a zero-truncated Poisson distribution.
707
708 *Presence/Absence model*
709 The presence/absence model makes several assumptions. We assume perfect detection of all
710 transmitted iSNV in the recipient. For each donor iSNV, we measure only whether or not the
711 variant is present in the recipient. Any iSNV that is not found in the recipient is assumed to have
712 not been transmitted. We also assume the probability of transmission is determined only by the
713 frequency of the iSNV in the donor at the time of sampling (regardless of how much time passes
714 between sampling and transmission). The probability of transmission is simply the probability
715 that the iSNV is included at least once in a sample size equal to the bottleneck. Finally, we
716 assume all genomic sites are independent of one another. For this reason, we discarded the
717 one case where the donor was likely infected by two strains, as the iSNV were certainly linked.
718
719 In our within host models, we only tracked minor alleles as in our data set we only ever find 2
720 alleles at each polymorphic site. In this case, the frequency of the major allele is simply one
721 minus the frequency of the minor allele. Because the presence/absence model is unaware of
722 the frequency of alleles in the recipient we must track both alleles at each donor polymorphic
723 site.
724
725 Let A_1 and A_2 be alleles in donor j at genomic site i. Let $P(A_1)$ be the probability that A_1 is the
726 only transmitted allele. There are three possible outcomes for each site. Either only A_1 is
727 transmitted, only A_2 is transmitted, or both A_1 and A_2 are transmitted. The probability of only A_1
728 being transmitted given a bottleneck size of N_b is

729

$$P_{i,j}(A_1 \mid N_b) = p_1^{N_b} \tag{11}$$

730

731 where p_1 is the frequency of A_1 in the donor. In other words, this is simply the probability of only

732 drawing A_1 in N_b draws. The probability that only A_2 is transmitted is similarly defined.

733

734 The probability of both alleles being transmitted is given by

735

$$P_{i,j}(A_1, A_2 \mid N_b) = 1 - (p_1^{N_b} + p_2^{N_b}) \tag{12}$$

736

737 where p_1 and p_2 are the frequencies of the alleles respectively. This is simply the probability of

738 not picking only A_1 or only A_2 in N_b draws.

739

740 This system could easily be extended to cases where there are more than 2 alleles present at a

741 site; however, that never occurs in our data set.

742

743 For ease we will denote the likelihood of observing the data at a polymorphic site i in each

744 donor j given the bottleneck size N_b as $P_{i,j}(N_b)$ where $P_{i,j}(N_b)$ is defined by equation 11 if only

745 one allele is transmitted and equation 12 if two alleles are transmitted.

746

747 The log likelihood of a bottleneck of size N_b is given by

748

$$LL(N_b) = \sum_j \sum_i \mathrm{Ln}\,(P_{i,j}) \tag{13}$$

749

750

where i, j refers to the ith polymorphic site in the jth donor. This is the log of the probability of observing the data summed over all polymorphic sites across all donors.

Because the bottleneck size is likely to vary across transmission events, we used maximum likelihood to fit the bottleneck distribution as oppose to fitting a single bottleneck value. Under this model we assumed the bottlenecks were distributed according to a zero-truncated Poisson distribution parameterized by λ. The likelihood of observing the data given a polymorphic site i in donor j and λ is

$$P_{i,j}(\lambda) = \sum_{N_b=1}^{\infty} P_{i,j}(N_b) P(N_b \mid \lambda) \quad (14)$$

where $P_{i,j}(N_b)$ is defined as above, $P(N_b \mid \lambda)$ is the probability of drawing a bottleneck of size N_b from a zero-truncated Poisson distribution with a mean of $\frac{\lambda}{1-e^{-\lambda}}$. The sum is across all possible N_b defined on $[1, \infty]$. For practical purposes, we only investigated bottleneck sizes up to 100, as initial analyses suggested λ is quite small and the probability of drawing a bottleneck size of 100 from a zero-truncated Poisson distribution with $\lambda = 10$ is negligible. We follow this convention whenever this sum appears.

The log likelihood of λ for the data set is given by

$$LL(\lambda) = \sum_{j} \sum_{i} \mathrm{Ln}\left(\sum_{N_b=1}^{\infty} P_{i,j}(N_b) P(N_b \mid \lambda) \right) \quad (15)$$

Beta Binomial model

The Beta binomial model is explained in detail in Leonard *et al.* (Sobel Leonard et al. 2017). It is similar to the presence/absence model in that transmission is modeled as a simple sampling process; however, it relaxes the following assumptions. In this model, the frequencies of transmitted variants are allowed to change between transmission and sampling according a beta distribution. The distribution is not dependent on the amount of time that passes between transmission and sampling, but rather depends on the size of the founding population (here assumed to equal to N_b) and the number of variant genomes present in founding population k. Note the frequency in the donor is assumed to be the same between sampling and transmission.

The equations below are very similar to those presented by Leonard *et al.* with one exception. Because we know the sensitivity of our method to detect rare variants based on the expected frequency and the titer, we can include the possibility that iSNV are transmitted but are missed due to poor sensitivity. Because the beta binomial model is aware of the frequency of the iSNV in the recipient, no information is added by tracking both alleles at a genomic site i.

Let p_{i,j_d} represent the frequency of the minor allele frequency at position i in the donor of some transmission pair j. Similarly, let p_{i,j_r} be the frequency of that same allele in the recipient of the jth transmission pair. Then, as in Leonard *et al.*, the likelihood of some bottleneck N_b for the data at site i in pair j where the minor allele is transmitted is given by

$$L(N_b)_{i,j} = \sum_{k=1}^{N_b} \text{p\_beta}\left(p_{i,j_r} \mid k, N_b - k\right) \text{p\_bin}\left(k \mid N_b, p_{i,j_d}\right) \quad (16)$$

Where p_beta is the probability density function for the beta distribution and p_bin is the probability mass function for the binomial distribution.

This is the probability density that the transmitted allele is found in the recipient at a frequency of p_{i,j_r} given that the variant was in k genomes in a founding population of size N_b times the probability of drawing k variant genomes in a sample size of N_b and a variant frequency of p_{i,j_d}. This is then summed for all possible k where $1 \leq k \leq N_b$.

As in equation 14 the likelihood of a zero truncated Poisson with a mean of $\frac{\lambda}{1-e^{-\lambda}}$ given this transmitted variants is then given by

$$L(\lambda)_{i,j}^{\text{transmitted}} = \sum_{N_b=1}^{\infty} L\,(N_b)_{i,j}\, P(N_b \mid \lambda) \tag{17}$$

This is simply the likelihood of each N_b weighted by the probability of drawing a bottleneck size of N_b from bottleneck distribution.

In this model, there are three possible mechanisms for a donor iSNV to not be detected in the recipient. (i) The variant was not transmitted. (ii) The variant was transmitted but is present below our level of detection (2%). (iii) The variant was transmitted and present above our level of detection but represents a false negative in iSNV identification.

As in Leonard *et al.*, the likelihood of scenarios (i) and (ii) for a given N_b are expressed as

$$L(N_b)_{i,j}^{\text{lost}} = \sum_{k=0}^{N_b} \text{p\_beta\_cdf}(p_{i,j_r} < 0.02 \mid k, N_b - k)\,\text{p\_bin}(k \mid N_b, p_{i,j_d})$$

(18)

Where p_beta_cdf is the cumulative distribution function for the beta distribution. Note that if $k = 0$ (i.e. the iSNV was not transmitted) then the term reduces to the probability of not drawing the variant in N_b draws.

The likelihood of the variant being transmitted but not detected in the recipient given a bottleneck of N_b is described by

$$L(N_b)_{i,j}^{\text{missed}} = \sum_{k=0}^{N_b} \sum_{f_e}^{[0.02,0.05,0.1)} \text{p\_beta\_cdf}(f_e < p_{i,j_r} < f_{e+1} \mid k, N_b - k) \times \text{p\_bin}(k \mid N_b, p_{i,j_d})(\text{FNR} \mid \text{Titer}_r, f_e) \quad (19)$$

This is the likelihood of the variant existing in the ranges [0.0.2,0.05] or [0.05,0.1] given an initial frequency of k/N_b and a bottleneck size of N_b multiplied by the expected false negative rate (FNR) given the titer of the recipient and the lower frequency bound. As in our diffusion model, we assumed perfect sensitivity for detection of iSNV present above 10%, rounded recipient titers down to the nearest $\log_{10}$ titer (e.g. 10^3,10^4, 10^5) and assumed the entire range $[f_e, f_{e+1}]$ has the same sensitivity as the lower bound.

The likelihood of λ for iSNV that are not observed in the recipient is then given by summing equations 18 and 19 across all possible N_b.

$$L(\lambda)_{i,j}^{\text{nontransmitted}} = \sum_{N_b=1}^{\infty} (L(N_b)_{i,j}^{\text{lost}} + L(N_b)_{i,j}^{\text{missed}}) P(N_b \mid \lambda) \quad (20)$$

The log likelihood of the total dataset is then determined by summing log of equations 17 and 20 (as applicable) across all polymorphic sites in each donor. (As before here we sum of N_b within the range $[1,100]$.)

Simulation

In order evaluate the fits of the two transmission models, we simulated whether or not each donor iSNV was transmitted or not. This involved converting each model to a presence absence model. In each simulation, we assigned a bottleneck from the bottleneck distribution for each transmission pair. We then determined the probability of only transmitting one allele (A_x where $x \in [1,2]$ as in the presence/absence model above) and the probability of transmitted both alleles (A_1, A_2 above) for each polymorphic site.

For the presence/absence model, the probabilities for each possible outcome are given by equations 11 and 12. For the beta binomial model, the probability of only observing A_x at site i is given by

$$P(A_x \mid N_b) = L(N_b)_{i,j}^{\text{lost}} + L(N_b)_{i,j}^{\text{missed}} \quad (21)$$

where $L(N_b)_{i,j}^{\text{lost}}$ and $L(N_b)_{i,j}^{\text{missed}}$ are defined as in equations 18 and 19 respectively, but with p_{i,j_d} replaced by $1 - p_{i,j_d}$. This is simply the probability of not observing the other allele in the recipient.

Again, the probability of observing both alleles is

$$P(A_1, A_2 \mid N_b) = 1 - (P(A_1) + P(A_2))$$

(22)

where $P(A_1)$ and $P(A_2)$ are defined as in equation 21.

Fitting mutation rate and N_e

The diffusion approximation to the Wright - Fischer model allows us to make predictions on the allele frequency spectrum of a population given a mutation rate and an effective population size. The probability of observing a mutation at frequency p_t given an initial frequency of 0 can be approximated as in (Rouzine et al. 2001)

$$P(0, p_t, t, \mid \mu, N_e) = \frac{2\mu N_e}{p_t} e^{-\frac{2N_e p_t}{t}}$$

(23)

Where μ is the mutation rate. In this model mutation increases an allele's frequency from 0 but after that initial jump, drift is responsible for allowing the mutation to reach it's observed frequency. Because the limit of equation 23 approaches infinity as p_t approaches 0 and for ease in numerical integration, we assumed that any variant present at less than 0.1% was essentially at 0%.

We then assumed each infection began as a clonal infection matching the consensus sequence observed at the time of sampling. The likelihood of observing minor alleles at the observed frequency is the given by equation 23.

As in the other within host models, we can account for nonpolymorphic sites by adding the likelihood that no mutation is present $P(0, p_t \approx 0, t \mid p_t < 0.001, \mu, N_e)$, that a mutation is present but below our level of detection $P(0, p_t \approx 0, t \mid p_t < 0.02, \mu, N_e)$, and that a mutation is present

887 but missed due to low sensitivity at low frequencies $P(0, p_t \approx 0, t \mid 0.02 < p_t < 0.1, \mu, N_e)$. In this
888 model we assumed 13133 mutagenic targets in each sample (the number of coding sites
889 present in the reference strain from 2014-2015).
890
891 The probability of not observing a mutation is given by
892

$$P(\,0, p_t \approx 0, t, \mid \mu, N_e\,) = P(\,0, p_t \approx 0, t \mid p_t < 0.001, \mu, N_e\,) +$$
893 $$P(\,0, p_t \approx 0, t \mid p_t < 0.02, \mu, N_e\,) +$$
894 $$P(0, p_t \approx 0, t \mid 0.02 < p_t < 0.1, \mu, N_e)$$
895 (24)

896 Where

$$P(0, p_t \approx 0, t \mid p_t < 0.001, \mu, N_e) = 1 - \int_{0.001}^{1} P\,(0, p_t, t, \mid \mu, N_e) dp_t$$

897 (25)

898 and

$$P(0, p_t \approx 0, t \mid p_t < 0.02, \mu, N_e) = \int_{0.001}^{0.02} P\,(0, p_t, t, \mid \mu, N_e) dp_t$$

899 (26)

900 and

$$P(0, p_t \approx 0, t \mid 0.02 < p_t < 0.1, \mu, N_e) = \sum_{f_i}^{[0.02, 0.05, 0.10)} (\,\mathrm{FNR} \mid \mathrm{Titer}_r, f_i) \int_{f_i}^{f_{i+1}} P\,(p_0, p_t, t \mid \mu, N_e) dp_t$$

901 (27)
902
903 Where we follow the same convention as in equation 5 for determining the false negative rate.
904 The log likelihood of a given μ and N_e pair is then the sum of the log of equations 23 and 24 for
905 all possible sites in the data set.
906

907 Annotated computer code for all analyses and for generating the figures can be accessed at

908 https://github.com/lauringlab/Host_level_IAV_evolution

909

910 **Acknowledgments**

911 This work was supported by a Clinician Scientist Development Award from the Doris Duke

912 Charitable Foundation (CSDA 2013105), a University of Michigan Discovery Grant, and R01

913 AI118886, all to ASL. The HIVE cohort was supported by NIH R01 AI097150 and CDC U01

914 IP00474 to ASM. JTM was supported by the Michigan Predoctoral Training Program in Genetics

915 (T32GM007544). RJW was supported by K08AI119182. We thank Alexey Kondrashov and

916 Aaron King for helpful discussion.

917

918 **References**

919 Alizon, S., Luciani, F. & Regoes, R.R., 2011. Epidemiological and clinical consequences of
920 within-host evolution. *Trends in microbiology*, 19(1), pp.24–32.

921 ARCHETTI, I. & HORSFALL, F.L., 1950. Persistent antigenic variation of influenza A viruses
922 after incomplete neutralization in ovo with heterologous immune serum. *The Journal of*
923 *experimental medicine*, 92(5), pp.441–462.

924 Caton, A.J. et al., 1982. The antigenic structure of the influenza virus A/PR/8/34 hemagglutinin
925 (H1 subtype). *Cell*, 31(2 Pt 1), pp.417–427.

926 Debbink, K. et al., 2017. Vaccination has minimal impact on the intrahost diversity of H3N2
927 influenza viruses. *PLoS pathogens*, 13(1), p.e1006194.

928 Dinis, J.M. et al., 2016. Deep Sequencing Reveals Potential Antigenic Variants at Low
929 Frequencies in Influenza A Virus-Infected Humans S. Schultz-Cherry, ed. *Journal of*
930 *Virology*, 90(7), pp.3355–3365.

931 Doud, M.B., Hensley, S.E. & Bloom, J.D., 2017. Complete mapping of viral escape from
932 neutralizing antibodies A. S. Lauring, ed. *PLoS pathogens*, 13(3), pp.e1006271–20.

933 Ewens, W.J., 2004. *Mathematical Population Genetics 1*, Springer Science & Business Media.

934 Flannery, B. et al., 2016. Enhanced Genetic Characterization of Influenza A(H3N2) Viruses and
935 Vaccine Effectiveness by Genetic Group, 2014-2015. *The Journal of Infectious Diseases*,
936 214(7), pp.1010–1019.

Foll, M. et al., 2014. Influenza virus drug resistance: a time-sampled population genetics perspective. *PLoS genetics*, 10(2), p.e1004185.

Foll, M., Shim, H. & Jensen, J.D., 2015. WFABC: a Wright-Fisher ABC-based approach for inferring effective population sizes and selection coefficients from time-sampled data. *Molecular ecology resources*, 15(1), pp.87–98.

Geoghegan, J.L., Senior, A.M. & Holmes, E.C., 2016. Pathogen population bottlenecks and adaptive landscapes: overcoming the barriers to disease emergence. *Proceedings. Biological sciences / The Royal Society*, 283(1837), pp.20160727–9.

Gerstung, M. et al., 2012. Reliable detection of subclonal single-nucleotide variants in tumour cell populations. *Nature Communications*, 3, p.811.

Ghedin, E. et al., 2011. Deep sequencing reveals mixed infection with 2009 pandemic influenza A (H1N1) virus strains and the emergence of oseltamivir resistance. *The Journal of Infectious Diseases*, 203(2), pp.168–174.

Gubareva, L.V. et al., 2001. Selection of influenza virus mutants in experimentally infected volunteers treated with oseltamivir. *The Journal of Infectious Diseases*, 183(4), pp.523–531.

Herfst, S. et al., 2012. Airborne transmission of influenza A/H5N1 virus between ferrets. *Science (New York, NY)*, 336(6088), pp.1534–1541.

Holmes, E.C., 2009. RNA virus genomics: a world of possibilities. *The Journal of clinical investigation*, 119(9), pp.2488–2495.

Hughes, J. et al., 2012. Transmission of equine influenza virus during an outbreak is characterized by frequent mixed infections and loose transmission bottlenecks. *PLoS pathogens*, 8(12), p.e1003081.

Iqbal, M. et al., 2009. Within-host variation of avian influenza viruses. *Philosophical transactions of the Royal Society of London Series B, Biological sciences*, 364(1530), pp.2739–2747.

Kao, R.R. et al., 2014. Supersize me: how whole-genomesequencing and big data aretransforming epidemiology. *Trends in microbiology*, pp.1–10.

Kimura, M., 1955. SOLUTION OF A PROCESS OF RANDOM GENETIC DRIFT WITH A CONTINUOUS MODEL. *Proceedings of the National Academy of Sciences of the United States of America*, 41(3), pp.144–150.

Kimura, M., 1971. Theoretical foundation of population genetics at the molecular level. *Theoretical population biology*, 2(2), pp.174–208.

Kimura, M. & Ohta, T., 1969. The Average Number of Generations until Fixation of a Mutant Gene in a Finite Population. *Genetics*, 61(3), pp.763–771.

Koel, B.F. et al., 2013. Substitutions near the receptor binding site determine major antigenic change during influenza virus evolution. *Science (New York, NY)*, 342(6161), pp.976–979.

Kouyos, R.D., Althaus, C.L. & Bonhoeffer, S., 2006. Stochastic or deterministic: what is the

973 effective population size of HIV-1? *Trends in microbiology*, 14(12), pp.507–511.

974 Kugelman, J.R. et al., 2017. Error baseline rates of five sample preparation methods used to
975 characterize RNA virus populations K. K. Tee, ed., 12(2), pp.e0171333–13. Available at:
976 http://dx.plos.org/10.1371/journal.pone.0171333.

977 Lee, M.-S. & Chen, J.S.-E., 2004. Predicting antigenic variants of influenza A/H3N2 viruses.
978 *Emerging infectious diseases*, 10(8), pp.1385–1390.

979 McCrone, J.T. & Lauring, A.S., 2016. Measurements of Intrahost Viral Diversity Are Extremely
980 Sensitive to Systematic Errors in Variant Calling. *Journal of Virology*, 90(15), pp.6884–6895.

981 Monto, A.S. et al., 2014. Frequency of acute respiratory illnesses and circulation of respiratory
982 viruses in households with children over 3 surveillance seasons. *The Journal of Infectious*
983 *Diseases*, 210(11), pp.1792–1799.

984 Murcia, P.R. et al., 2010. Intra- and interhost evolutionary dynamics of equine influenza virus.
985 *Journal of Virology*, 84(14), pp.6943–6954.

986 Myers, S., Fefferman, C. & Patterson, N., 2008. Can one learn history from the allelic spectrum?
987 *Theoretical population biology*, 73(3), pp.342–348.

988 Neher, R.A. & Bedford, T., 2015. nextflu: real-time tracking of seasonal influenza virus evolution
989 in humans. *Bioinformatics (Oxford, England)*, p.btv381.

990 Nelson, M.I. & Holmes, E.C., 2007. The evolution of epidemic influenza. *Nature Reviews*
991 *Genetics*, 8(3), pp.196–205.

992 Nelson, M.I. et al., 2006. Stochastic processes are key determinants of short-term evolution in
993 influenza a virus. *PLoS pathogens*, 2(12), p.e125.

994 Ohmit, S.E. et al., 2015. Influenza vaccine effectiveness in households with children during the
995 2012-2013 season: assessments of prior vaccination and serologic susceptibility. *The*
996 *Journal of Infectious Diseases*, 211(10), pp.1519–1528.

997 Ohmit, S.E. et al., 2013. Influenza Vaccine Effectiveness in the Community and the Household.
998 *Clinical infectious diseases : an official publication of the Infectious Diseases Society of*
999 *America*, 56(10), pp.1363–1369.

1000 Ohmit, S.E. et al., 2016. Substantial Influenza Vaccine Effectiveness in Households With
1001 Children During the 2013-2014 Influenza Season, When 2009 Pandemic Influenza A(H1N1)
1002 Virus Predominated. *The Journal of Infectious Diseases*, 213(8), pp.1229–1236.

1003 Pauly, M.D., Procario, M.C. & Lauring, A.S., 2017. A novel twelve class fluctuation test reveals
1004 higher than expected mutation rates for influenza A viruses. *eLife*, 6, p.e26437.

1005 Peck, K.M., Chan, C.H.S. & Tanaka, M.M., 2015. Connecting within-host dynamics to the rate of
1006 viral molecular evolution. *Virus Evolution*, 1(1), p.vev013.

1007 Petrie, J.G. et al., 2017. Application of an Individual-Based Transmission Hazard Model for
1008 Estimation of Influenza Vaccine Effectiveness in a Household Cohort. *American journal of*

epidemiology.

Petrie, J.G. et al., 2013. Influenza Transmission in a Cohort of Households with Children: 2010-2011 J. McVernon, ed. *PLoS ONE*, 8(9), p.e75339.

Petrova, V.N. & Russell, C.A., 2017. The evolution of seasonal influenza viruses. *Nature Reviews Microbiology*, 2, p.517.

Poon, L.L.M. et al., 2016. Quantifying influenza virus diversity and transmission in humans. *Nature Genetics*, 48(2), pp.195–200.

Rambaut, A. et al., 2008. The genomic and epidemiological dynamics of human influenza A virus. *Nature*, 453(7195), pp.615–619.

Rogers, M.B. et al., 2015. Intrahost dynamics of antiviral resistance in influenza A virus reflect complex patterns of segment linkage, reassortment, and natural selection. *mBio*, 6(2).

Rouzine, I.M., Rodrigo, A. & Coffin, J.M., 2001. Transition between stochastic evolution and deterministic evolution in the presence of selection: general theory and application to virology. *Microbiology and molecular biology reviews : MMBR*, 65(1), pp.151–185.

Russell, C.A. et al., 2012. The potential for respiratory droplet-transmissible A/H5N1 influenza virus to evolve in a mammalian host. *Science (New York, NY)*, 336(6088), pp.1541–1547.

Sanjuán, R. et al., 2010. Viral mutation rates. *Journal of Virology*, 84(19), pp.9733–9748.

Smith, D.J. et al., 2004. Mapping the antigenic and genetic evolution of influenza virus. *Science (New York, NY)*, 305(5682), pp.371–376.

Sobel Leonard, A. et al., 2016. Deep Sequencing of Influenza A Virus from a Human Challenge Study Reveals a Selective Bottleneck and Only Limited Intrahost Genetic Diversification D. S. Lyles, ed. *Journal of Virology*, 90(24), pp.11247–11258.

Sobel Leonard, A. et al., 2017. Transmission Bottleneck Size Estimation from Pathogen Deep-Sequencing Data, with an Application to Human Influenza A Virus. *Journal of Virology*, 91(14).

Varble, A. et al., 2014. Influenza A virus transmission bottlenecks are defined by infection route and recipient host. *Cell Host and Microbe*, 16(5), pp.691–700.

Visher, E. et al., 2016. The Mutational Robustness of Influenza A Virus N. M. Ferguson, ed. *PLoS pathogens*, 12(8), pp.e1005856–25.

Wiley, D.C., Wilson, I.A. & Skehel, J.J., 1981. Structural identification of the antibody-binding sites of Hong Kong influenza haemagglutinin and their involvement in antigenic variation. *Nature*, 289(5796), pp.373–378.

Wilker, P.R. et al., 2013. Selection on haemagglutinin imposes a bottleneck during mammalian transmission of reassortant H5N1 influenza viruses. *Nature Communications*, 4, p.2636.

Williamson, E.G. & Slatkin, M., 1999. Using maximum likelihood to estimate population size from temporal changes in allele frequencies. *Genetics*, 152(2), pp.755–761.

1045 Xu, R. et al., 2010. Structural basis of preexisting immunity to the 2009 H1N1 pandemic
1046 influenza virus. *Science (New York, NY)*, 328(5976), pp.357–360.

1047 Xue, K.S. et al., 2017. Parallel evolution of influenza across multiple spatiotemporal scales.
1048 *eLife*, 6, p.e26875.

1049 Zanini, F. et al., 2017. In vivo mutation rates and the landscape of fitness costs of HIV-1. *Virus*
1050 *Evolution*, 3(1), p.vex003.

1051 Zhou, B. et al., 2009. Single-reaction genomic amplification accelerates sequencing and vaccine
1052 production for classical and Swine origin human influenza a viruses. *Journal of Virology*,
1053 83(19), pp.10309–10313.

1054 Zwart, M.P. & Elena, S.F., 2015. Matters of Size: Genetic Bottlenecks in Virus Infection and
1055 Their Potential Impact on Evolution. *Annual Review of Virology*, 2(1), pp.161–179.

1056

1057

Figure Legends

Figure 1. Within host diversity of IAV populations. (A) Boxplots (median, 25th and 75th percentiles, whiskers extend to most extreme point within median ± 1.5 x IQR) of the number of viral genomes per microliter transport media stratified by day post symptom onset. Notches represent the approximate 95% confidence interval of the median. (B) Boxplots (median, 25th and 75th percentiles, whiskers extend to most extreme point within median ± 1.5 x IQR) of the number of iSNV in 249 high quality samples stratified by day post symptom onset. (C) Histogram of within host iSNV frequency in 249 high quality samples. Bin width is 0.05 beginning at 0.02. Mutations are colored nonsynonymous (blue) and synonymous (gold) (D) Location of all identified iSNV in the influenza A genome. Mutations are colored nonsynonymous (blue) and synonymous (gold) relative to that sample's consensus sequence. Triangles signify mutations that were found in more than one individual in a given season.

Figure 2. Within host dynamics of IAV. (A) Timing of sample collection for 35 paired longitudinal samples relative to day of symptom onset. Of the 49 total, 35 pairs had minor iSNV present in the first sample. (B) The change in frequency over time for minority nonsynonymous (blue) and synonymous (gold) iSNV identified for the paired samples in (A). (C) The distribution of effective population sizes estimated from 1,000 simulated populations. Simulations were run on populations with characteristics similar to the actual patient-derived populations and with the specified effective population size (x-axis). (D) The effect of iteratively removing iSNV with the most extreme change in frequency (fraction of iSNV removed, x-axis) on the estimated effective population size. The point represents the estimate when all iSNV are included. (E) The posterior distributions of selection coefficients estimated for the 35 iSNV present in isolates sampled one day apart. Distributions are colored according to class relative to the sample consensus sequence, nonsynonymous (blue) synonymous (gold). Variants for which the 95% highest

1083 posterior density intervals exclude 0.0 are noted in the margin.

1084

1085 **Figure 3.** Between host dynamics of IAV. (A) The distribution of pairwise L1-norm distances for
1086 household (blue) and randomly-assigned community (gold) pairs. The bar heights are
1087 normalized to the height of the highest bar for each given subset (47 for household, 1,592 for
1088 community). The red line represents the 5th percentile of the community distribution. (B) Timing
1089 of symptom onset for 52 epidemiologically linked transmission pairs. Day of symptom onset for
1090 both donor and recipient individuals is indicated by black dots. Dashed lines represent pairs that
1091 were removed due to abnormally high genetic distance between isolates, see (A). (C) The
1092 frequency of donor iSNV in both donor and recipient samples. Frequencies below 2% and
1093 above 98% were set to 0% and 100% respectively. (D) The presence-absence model fit
1094 compared with the observed data. The x-axis represents the frequency of donor iSNV with
1095 transmitted iSNV plotted along the top and nontransmitted iSNV plotted along the bottom. The
1096 black line indicates the probability of transmission for a given iSNV frequency as determined by
1097 logistic regression. Similar fits were calculated for 1,000 simulations with a mean bottleneck size
1098 of 1.66. Fifty percent of simulated outcomes lie in the darkly shaded region and 95% lie in the
1099 lightly shaded regions. (E) The outcome from 1,000 simulated “transmission” events with
1100 randomly assigned pairings. The black line represents the observed data, as in (D) the shaded
1101 regions represent the middle 50% and 95% of simulated outcomes. The results from the
1102 simulated logit models were smoothed by plotting the predicted probability of transmission at
1103 0.02 intervals. (F) The beta-binomial model fit. Similar to (D) except the simulated outcomes are
1104 the based on a beta-binomial model using a mean bottleneck of 1.73.

1105

1106 **Figure 4.** Combined estimates of within host mutation rate and effective population size.
1107 Contour plot shows the log likelihood surface for estimates of the effective population size and

neutral mutation rate. The point represents the peak ($\mu = 4x10^{-6}$, $N_e = 36$, log likelihood = -4,687). Log likelihoods for each contour are indicated.

Supplementary Figure 1. Sequence coverage for all samples. For each sample, the sliding window mean coverage was calculated using a window size of 200 and a step of 100. The distributions of these means are plotted as box plots (median, 25th and 75th percentiles, whiskers extend to most extreme point within median ± 1.5 x IQR) where the y-axis represents the read depth and the x-axis indicates the position of the window in a concatenated IAV genome.

Supplementary Figure 2. Approximate maximum likelihood trees of the concatenated coding sequences for high quality H1N1 samples. The branches are colored by season; the tip identifiers are colored by household. Arrows with numbers indicate consensus and putative minor haplotypes for samples with greater than 10 iSNV. Trees were made using FastTree.

Supplementary Figure 3. Approximate maximum likelihood trees of the concatenated coding sequences for high quality H3N2 samples. The branches are colored by season; the tip identifiers are colored by household. Arrows with numbers indicate consensus and putative minor haplotypes for samples with greater than 10 iSNV. Trees were made using FastTree.

Supplementary Figure 4. The effect of titer and vaccination on the number of iSNV identified. (A) The number of iSNV identified in an isolate (y-axis) plotted against the titer (x-axis, genomes/µl transport media). (B) The number of iSNV identified in each isolate stratified by whether that individual was vaccinated or not. Red bars indicate the median of each distribution.

Supplementary Figure 5. Minority nonsynonymous iSNV in global circulation.

1134 The global frequencies of the amino acids that were found as minority variants in sample
1135 isolates (x-axis) plotted overtime (y-axis). Each amino acid trace is labeled according to the H3
1136 number scheme. All samples were isolated in December of 2014 (gray line).
1137
1138 **Supplementary Figure 6.** Reproducibility of iSNV identification for paired samples acquired on
1139 the same day. The x-axis represents iSNV frequencies found in the home-acquired nasal swab.
1140 The y-axis represents iSNV frequencies found the clinic-acquired combined throat and nasal
1141 swab.
1142
1143 **Supplementary Figure 7.** Estimate of effective bottleneck size with relaxed variant calling
1144 criteria. (A) The frequency of iSNV in both recipient and donor isolates. iSNV were identified
1145 using the original variant calling pipeline. (B) The presence-absence model fit compared to the
1146 observed data for iSNV identified using the original variant calling pipeline. The x-axis
1147 represents the frequency of donor iSNV with transmitted iSNV plotted along the top and
1148 nontransmitted iSNV plotted along the bottom. The black line indicates the probability of
1149 transmission for a given iSNV frequency as determined by logistic regression. Similar fits were
1150 calculated for 1,000 simulations with a mean bottleneck size of 2.10. Fifty percent of simulated
1151 outcomes lie in the darkly shaded region and 95% lie in the lightly shaded regions. (C) Similar to
1152 (A) but with minority iSNV identified using the current analytical framework without a frequency
1153 threshold. (D) Similar to B but with minority iSNV identified using the current analytical
1154 framework without a frequency threshold.
1155

Table 1. Influenza viruses over five seasons in a household cohort

	2010-2011	2011-2012	2012-2013	2013-2014	2014-2015
Households	328	213	321	232	340
Participants	1441	943	1426	1049	1431
Vaccinated, n (%)[a]	934 (65)	554 (59)	942 (66)	722 (69)	992 (69)
IAV Positive Individuals[b]	86	23	69	48	166
H1N1	26	1	3	47	0
H3N2	58	22	66	1	166
IAV Positive Households[c]					
Two individuals	13	2	9	7	23
Three individuals	5	2	3	3	11
Four individuals	-	-	1	2	4
High Quality NGS Pairs[d]	4	1	2	6	39

[a] Self reported or confirmed receipt of vaccine prior to the specified season.
[b] RT-PCR confirmed infection.
[c] Households in which two individuals were positive within 7 days of each other. In cases of trios and quartets, the putative chains could have no pair with onset >7 days apart.
[d] Samples with $>10^3$ genome copies per µl of transport medium, adequate amplification of all 8 genomic segments, and average sequencing coverage $>10^3$ per nucleotide.

Table 2. Within host effective population size of IAV

Model	SNV Used	Generation Time (h)	Effective Population Size (95% CI)
Diffusion approximation	All	6	35 (26-46)
	All	12	17 (13-23)
Discrete model	All	6	32 (28-41)
	Nonsynonymous	6	30 (21-40)
	Synonymous	6	37 (27-54)
	All	12	23 (23-29)
	Nonsynonymous	12	19 (19-21)
	Synonymous	12	27 (22-33)

Supplementary Table 1. Sensitivity and specificity of variant detection

Copy Number[a]	Variant Frequency	Original Pipeline[b]		Current Pipeline[c]	
		Sensitivity	Specificity	Sensitivity	Specificity
$>10^5$	0.05	1	>0.9999	0.85	1.000
	0.02	0.85	0.9999	0.15	1.000
	0.01	0.95	0.9995	-	-
	0.005	0.35	0.9999	-	-
10^4-10^5	0.05	0.95	0.9999	0.85	1.000
	0.02	0.9	0.9999	0.15	1.000
	0.01	0.8	0.9998	-	-
	0.005	0.4	0.9999	-	-
10^3-10^4	0.05	0.8	>0.9999	0.70	1.000
	0.02	0.45	0.9999	0.15	1.000
	0.01	0.2	0.9997	-	-
	0.005	0.1	0.9999	-	-

[a] Per µl transport media
[b] As described in McCrone JT and Lauring AS, J. Virol. 90(15):6884, 2016.
[c] As described in Methods, benchmarked for frequencies 0.02-0.98 only

Supplementary Table 2. Nonsynonymous substitutions in HA antigenic sites

House ID	Enrolment ID	Symptom Onset	Subtype	Frequency	Amino Acid Change	Antigenic Site	Vaccinated	Day of Symptoms
1111	300481	3-30-2011	H3N2	0.071	E62G	E*	No	0
2166	320661	2-13-2012	H3N2	0.071	V297A	C	Yes	1
1302	301355	3-20-2011	H3N2	0.088	L86I	E	Yes	1
3075	331045	12-10-2012	H3N2	0.066	I214T	D	Yes	1
5219	50935	12-5-2014	H3N2	0.175	F193S	B*†	No	3
5263	51106	12-6-2014	H3N2	0.111	T128A	B	Yes	3
5290	51225	12-15-2014	H3N2	0.405	I260V	E*	Yes	1
5302	51273	12-13-2014	H3N2	0.030	S262N	E*	Yes	0
5098	50419	12-22-2014	H3N2	0.364	G208R	D	Yes	4
5033	50141	12-3-2014	H3N2	0.032	A163T	B	Yes	2
5034	50143	1-11-2015	H3N2	0.119	I307R	C	Yes	1
5289	51220	12-13-2014	H3N2	0.038	K189N	B*†	Yes	-1
5033	50141	12-3-2014	H3N2	0.025	D53E	C*	Yes	1
5033	50141	12-3-2014	H3N2	0.023	S312G	C	Yes	1
5269	51132	12-6-2014	H3N2	0.028	I242T	D	Yes	2
5147	50630	11-18-2014	H3N2	0.164	I242L	D	Yes	1
5034	50143	1-11-2015	H3N2	0.161	I307R	C	Yes	2
4185	UM40738	12-14-2013	H1N1	0.021	R208K	Ca	No	2

* Sites observed to vary between antigenically distinct strains in Wiley et al., 1981 and Smith DJ et al., 2004.
† Sites located in the “antigenic ridge” identified in Koel et al., 2013.

Figure 1

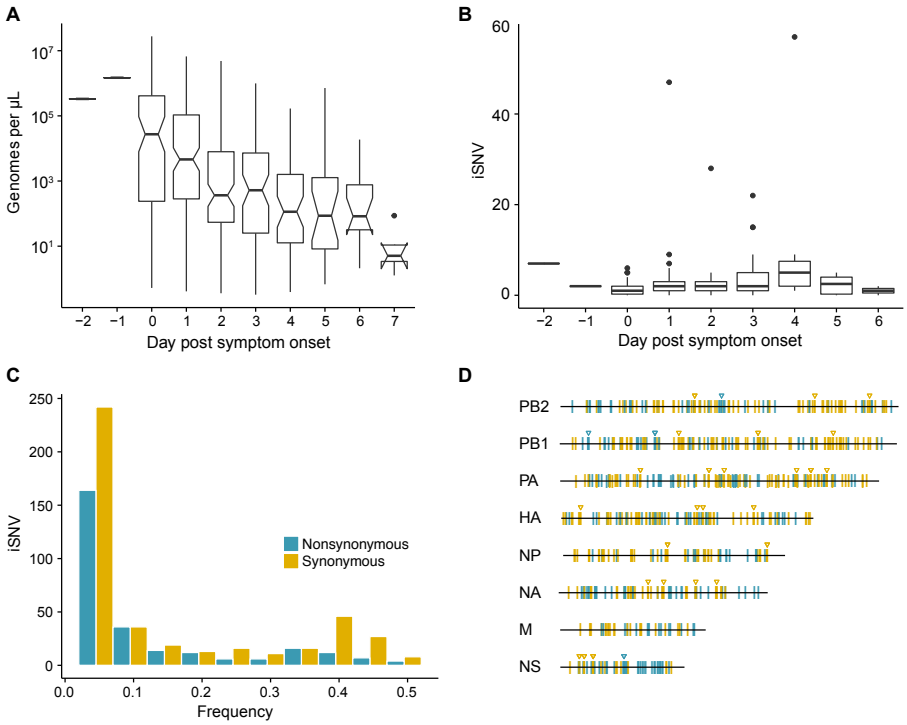

Figure 1. Within host diversity of IAV populations. (A) Boxplots (median, 25th and 75th percentiles, whiskers extend to most extreme point within median ± 1.5 x IQR) of the number of viral genomes per microliter transport media stratified by day post symptom onset. Notches represent the approximate 95% confidence interval of the median. (B) Boxplots (median, 25th and 75th percentiles, whiskers extend to most extreme point within median ± 1.5 x IQR) of the number of iSNV in 249 high quality samples stratified by day post symptom onset. (C) Histogram of within host iSNV frequency in 249 high quality samples. Bin width is 0.05 beginning at 0.02. Mutations are colored nonsynonymous (blue) and synonymous (gold) (D) Location of all identified iSNV in the influenza A genome. Mutations are colored nonsynonymous (blue) and synonymous (gold) relative to that sample's consensus sequence. Triangles signify mutations that were found in more than one individual in a given season.

Figure 2

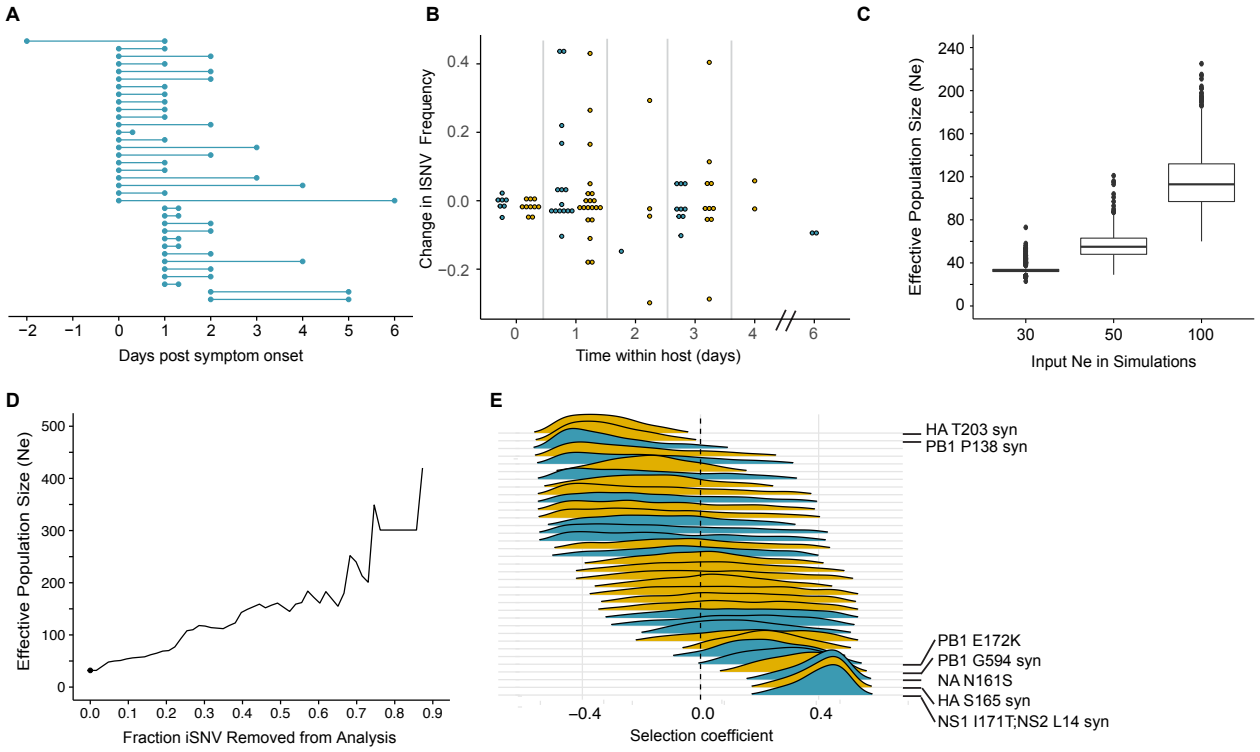

Figure 2. Within host dynamics of IAV. (A) Timing of sample collection for 35 paired longitudinal samples relative to day of symptom onset. Of the 49 total, 35 pairs had minor iSNV present in the first sample. (B) The change in frequency over time for minority nonsynonymous (blue) and synonymous (gold) iSNV identified for the paired samples in (A). (C) The distribution of effective population sizes estimated from 1,000 simulated populations. Simulations were run on populations with characteristics similar to the actual patient-derived populations and with the specified effective population size (x-axis). (D) The effect of iteratively removing iSNV with the most extreme change in frequency (fraction of iSNV removed, x-axis) on the estimated effective population size. The point represents the estimate when all iSNV are included. (E) The posterior distributions of selection coefficients estimated for the 35 iSNV present in isolates sampled one day apart. Distributions are colored according to class relative to the sample consensus sequence, nonsynonymous (blue) synonymous (gold). Variants for which the 95% highest posterior density intervals exclude 0.0 are noted in the margin.

Figure 3

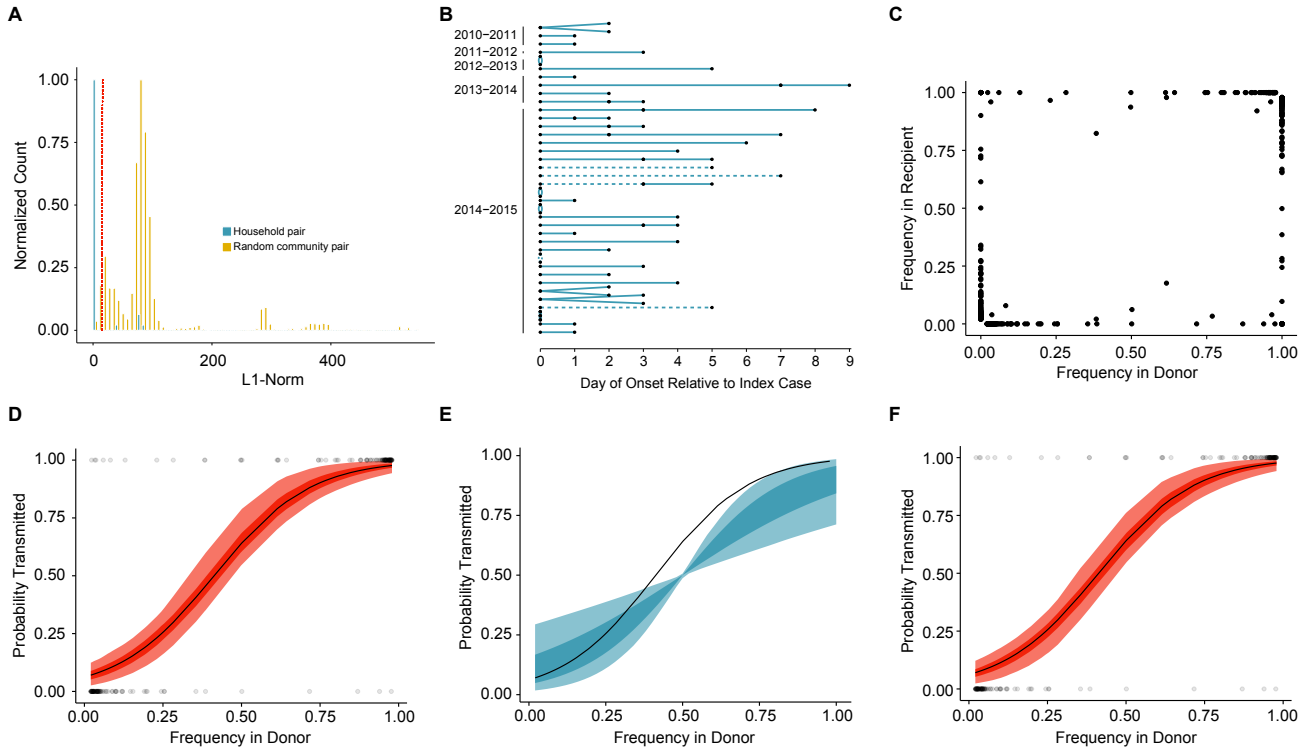

Figure 3. Between host dynamics of IAV. (A) The distribution of pairwise L1-norm distances for household (blue) and randomly-assigned community (gold) pairs. The bar heights are normalized to the height of the highest bar for each given subset (47 for household, 1,592 for community). The red line represents the 5th percentile of the community distribution. (B) Timing of symptom onset for 52 epidemiologically linked transmission pairs. Day of symptom onset for both donor and recipient individuals is indicated by black dots. Dashed lines represent pairs that were removed due to abnormally high genetic distance between isolates, see (A). (C) The frequency of donor iSNV in both donor and recipient samples. Frequencies below 2% and above 98% were set to 0% and 100% respectively. (D) The presence-absence model fit compared with the observed data. The x-axis represents the frequency of donor iSNV with transmitted iSNV plotted along the top and nontransmitted iSNV plotted along the bottom. The black line indicates the probability of transmission for a given iSNV frequency as determined by logistic regression. Similar fits were calculated for 1,000 simulations with a mean bottleneck size of 1.66. Fifty percent of simulated outcomes lie in the darkly shaded region and 95% lie in the lightly shaded regions. (E) The outcome from 1,000 simulated “transmission” events with randomly assigned pairings. The black line represents the observed data, as in (D) the shaded regions represent the middle 50% and 95% of simulated outcomes. The results from the simulated logit models were smoothed by plotting the predicted probability of transmission at 0.02 intervals. (F) The beta-binomial model fit. Similar to (D) except the simulated outcomes are the based on a beta-binomial model using a mean bottleneck of 1.73.

Figure 4

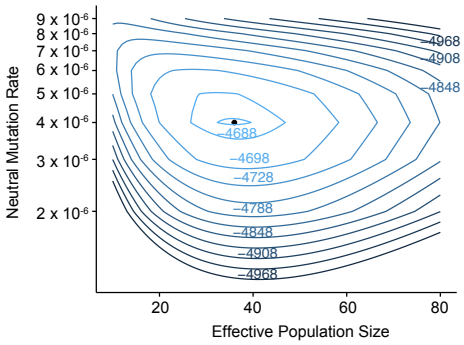

Figure 4. Combined estimates of within host mutation rate and effective population size. Contour plot shows the log likelihood surface for estimates of the effective population size and neutral mutation rate. The point represents the peak (μ = 4x10-6, Ne = 36, log likelihood = -4,687). Log likelihoods for each contour are indicated.

Supplementary Figure 1

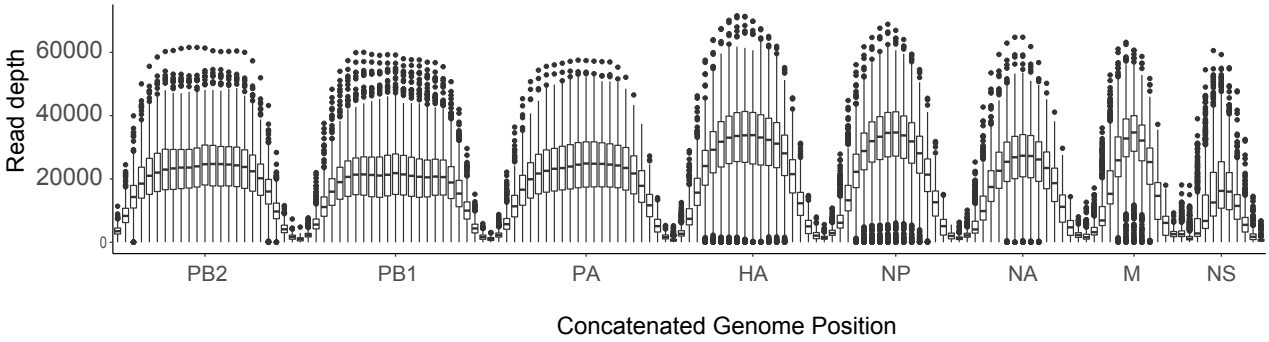

Supplementary Figure 1. Sequence coverage for all samples. For each sample, the sliding window mean coverage was calculated using a window size of 200 and a step of 100. The distributions of these means are plotted as box plots (median, 25th and 75th percentiles, whiskers extend to most extreme point within median ± 1.5 x IQR) where the y-axis represents the read depth and the x-axis indicates the position of the window in a concatenated IAV genome.

Supplementary Figure 2

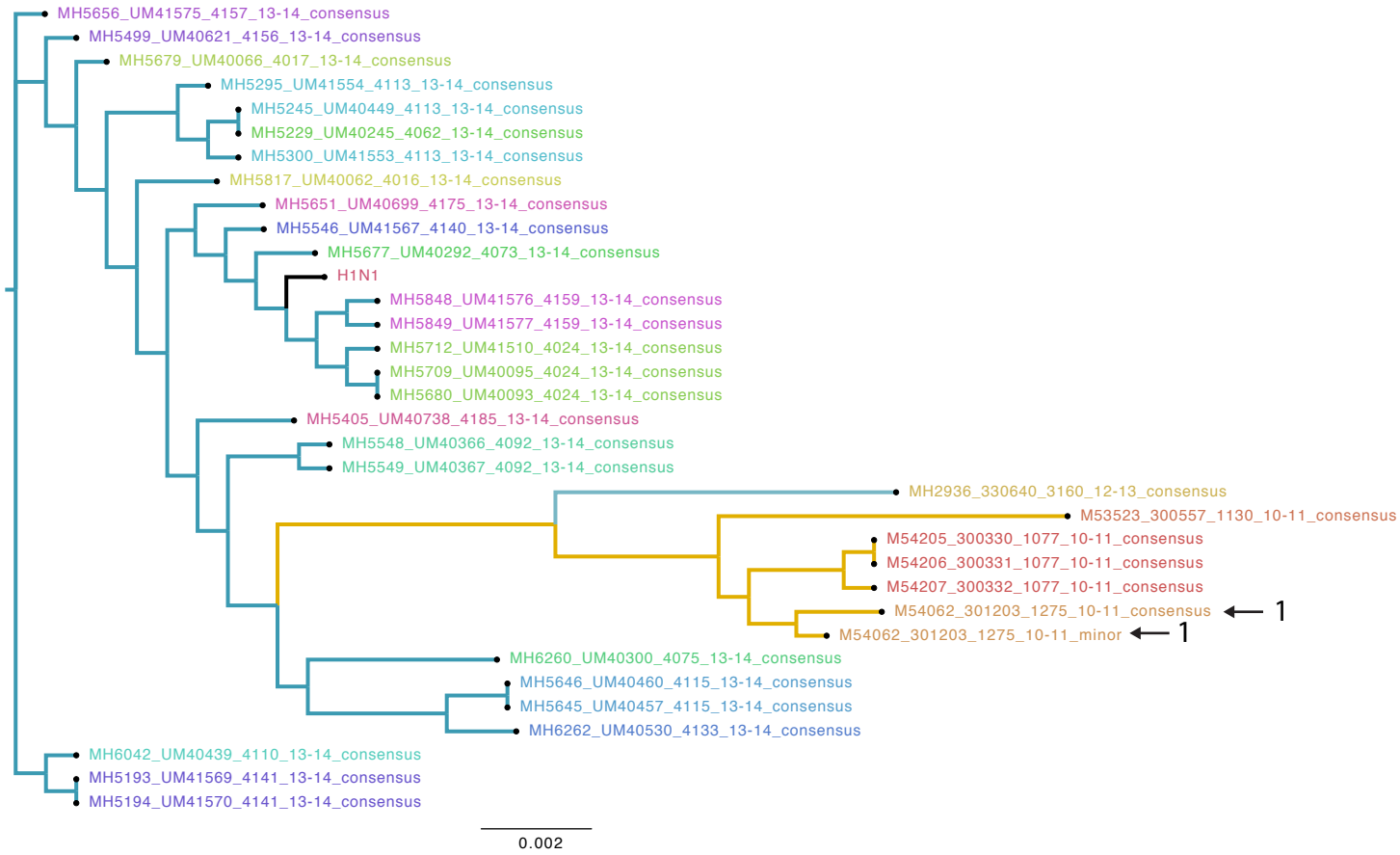

Supplementary Figure 2. Approximate maximum likelihood trees of the concatenated coding sequences for high quality H1N1 samples. The branches are colored by season; the tip identifiers are colored by household. Arrows with numbers indicate consensus and putative minor haplotypes for samples with greater than 10 iSNV. Trees were made using FastTree.

Supplementary Figure 3

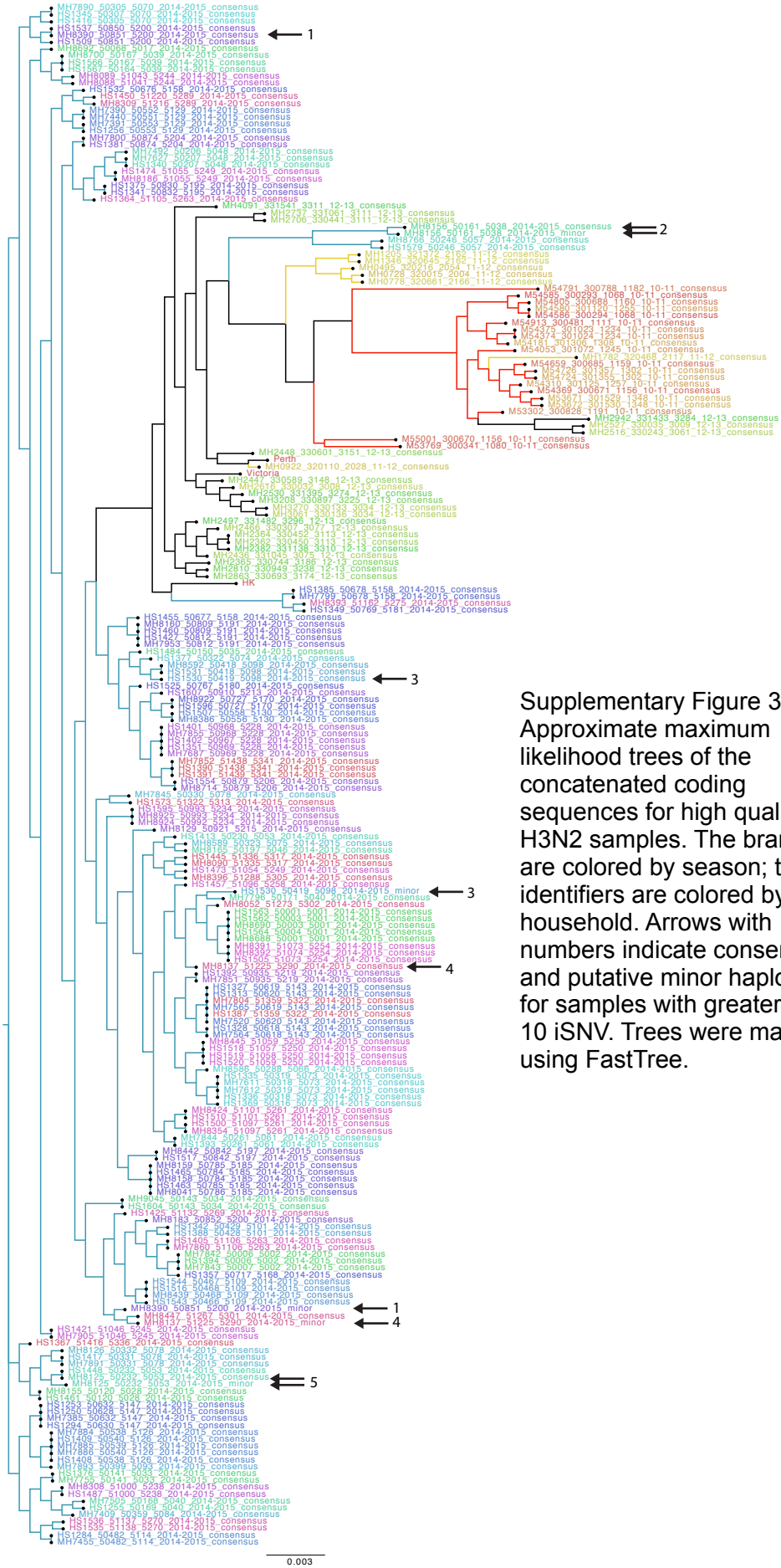

Supplementary Figure 3. Approximate maximum likelihood trees of the concatenated coding sequences for high quality H3N2 samples. The branches are colored by season; the tip identifiers are colored by household. Arrows with numbers indicate consensus and putative minor haplotypes for samples with greater than 10 iSNV. Trees were made using FastTree.

Supplementary Figure 4

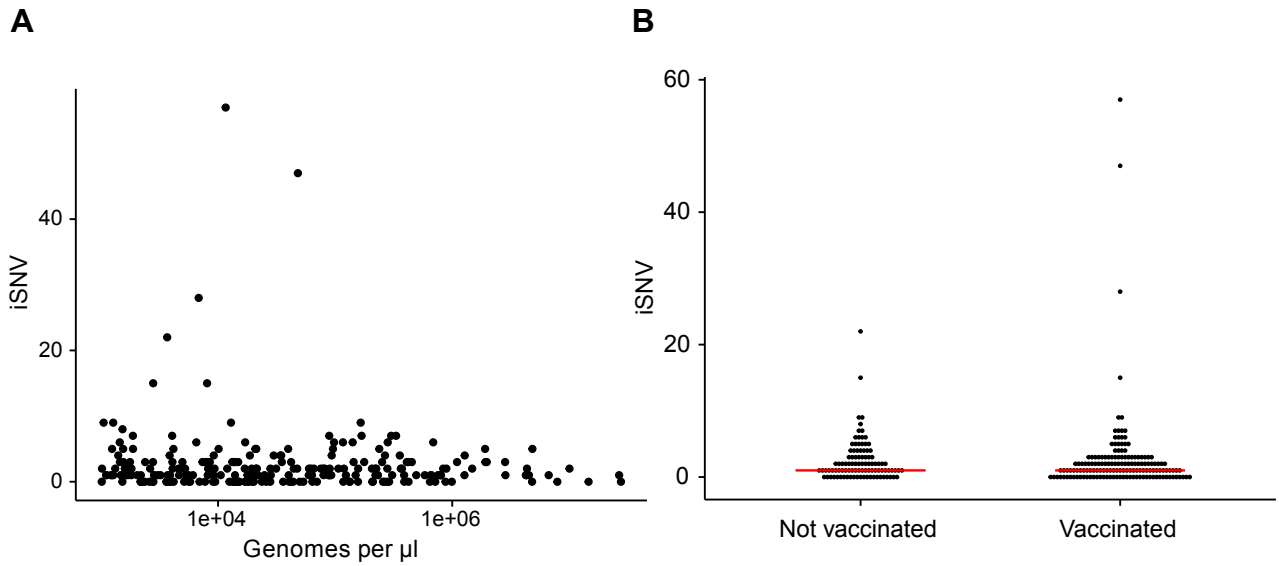

Supplementary Figure 4. The effect of titer and vaccination on the number of iSNV identified. (A) The number of iSNV identified in an isolate (y-axis) plotted against the titer (x-axis, genomes/µl transport media). (B) The number of iSNV identified in each isolate stratified by whether that individual was vaccinated or not. Red bars indicate the median of each distribution.

Supplementary Figure 5

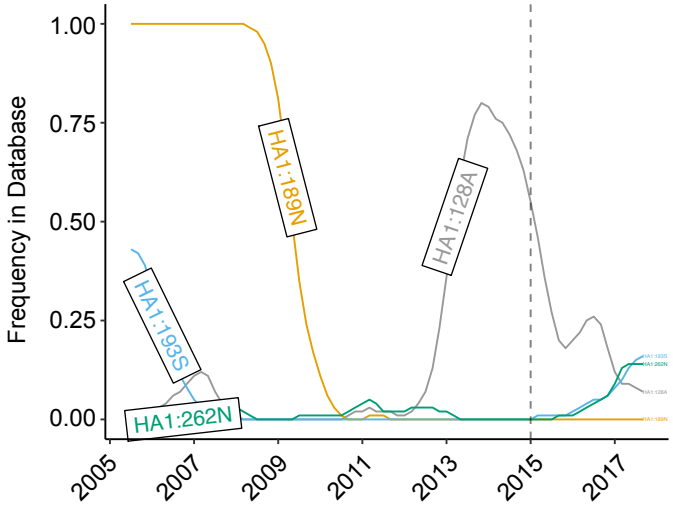

Supplementary Figure 5. Minority nonsynonymous iSNV in global circulation. The global frequencies of the amino acids that were found as minority variants in sample isolates (x-axis) plotted overtime (y-axis). Each amino acid trace is labeled according to the H3 number scheme. All samples were isolated in December of 2014 (gray line).

Supplementary Figure 6

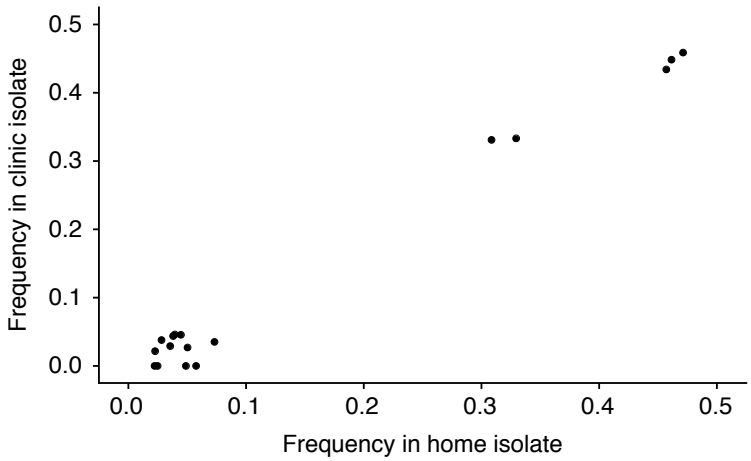

Supplementary Figure 6. Reproducibility of iSNV identification for paired samples acquired on the same day. The x-axis represents iSNV frequencies found in the home-acquired nasal swab. The y-axis represents iSNV frequencies found the clinic-acquired combined throat and nasal swab.

Supplementary Figure 7

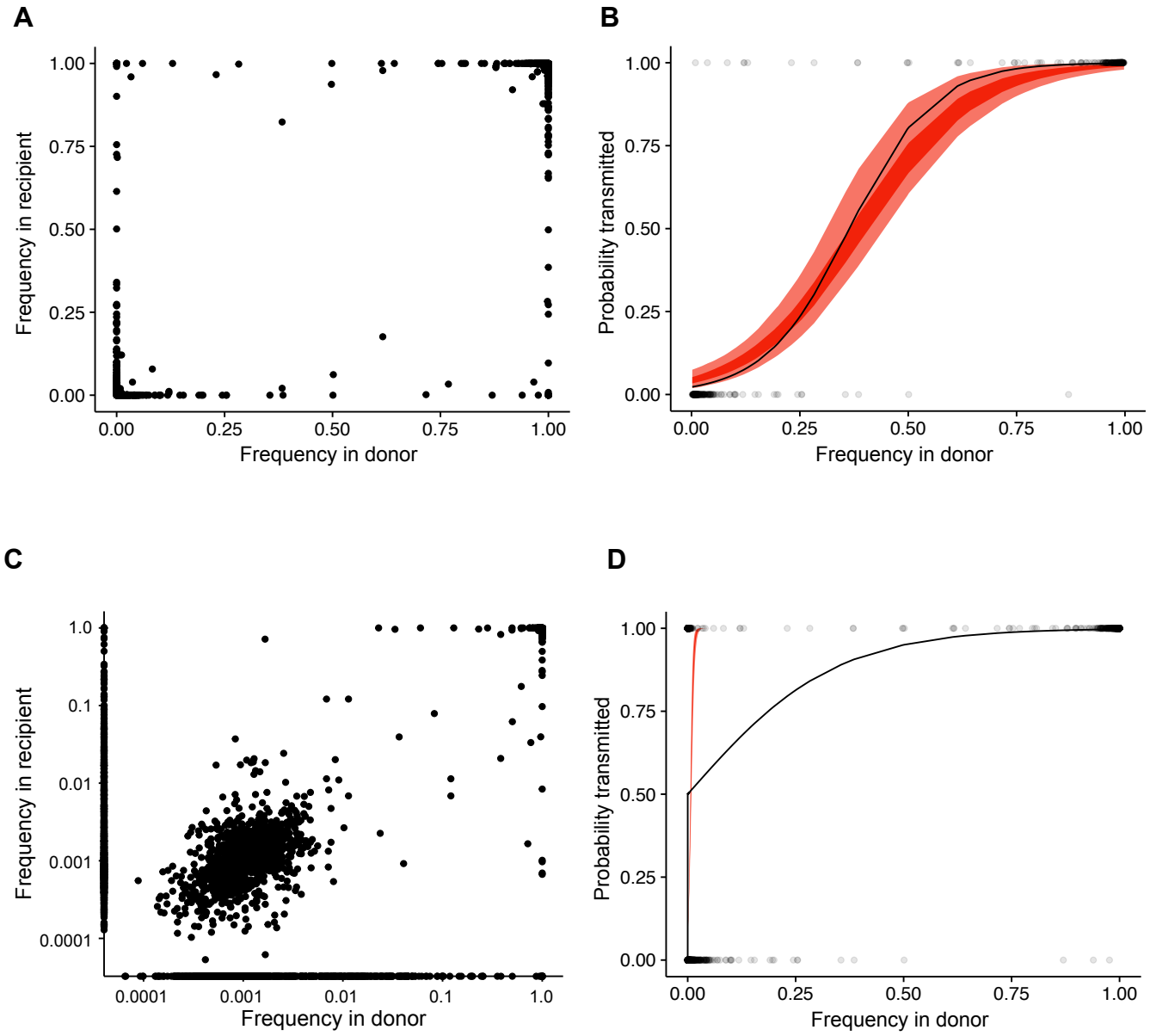

Supplementary Figure 7. Estimate of effective bottleneck size with relaxed variant calling criteria. (A) The frequency of iSNV in both recipient and donor isolates. iSNV were identified using the original variant calling pipeline. (B) The presence-absence model fit compared to the observed data for iSNV identified using the original variant calling pipeline. The x-axis represents the frequency of donor iSNV with transmitted iSNV plotted along the top and nontransmitted iSNV plotted along the bottom. The black line indicates the probability of transmission for a given iSNV frequency as determined by logistic regression. Similar fits were calculated for 1,000 simulations with a mean bottleneck size of 2.10. Fifty percent of simulated outcomes lie in the darkly shaded region and 95% lie in the lightly shaded regions. (C) Similar to (A) but with minority iSNV identified using the current analytical framework without a frequency threshold. (D) Similar to B but with minority iSNV identified using the current analytical framework without a frequency threshold.